ISSN 1674-1056
http://cpb.iphy.ac.cn
http://iopscience.iop.org/cpb
中国物理 B
Chinese Physics
中国物理 Chinese Physics B

Review of deep ultraviolet photodetector based on gallium oxide

Yuan Qin(覃愿), Shibing Long(龙世兵), Hang Dong(董航), Qiming He(何启鸣), Guangzhong Jian(菅光忠), Ying Zhang(张颖), Xiaohu Hou(侯小虎), Pengju Tan(谭鹏举), Zhongfang Zhang(张中方), Hangbing Lv(吕杭炳), Qi Liu(刘琦), Ming Liu(刘明)

Citation: Chin. Phys. B . 2019, 28(1): 018501. **doi:** 10.1088/1674-1056/28/1/018501
Journal homepage: http://cpb.iphy.ac.cn; http://iopscience.iop.org/cpb

What follows is a list of articles you may be interested in

Electronic synapses based on ultrathin quasi-two-dimensional gallium oxide memristor

Shuopei Wang(王硕培), Congli He(何聪丽), Tang Jian(汤建), Rong Yang(杨蓉), Dongxia Shi(时东霞), Guangyu Zhang(张广宇)

Chin. Phys. B . 2019, 28(1): 017304. **doi:** 10.1088/1674-1056/28/1/017304

Photon-counting chirped amplitude modulation lidar system using superconducting nanowire single-photon detector at 1550-nm wavelength

Hui Zhou(周慧), Yu-Hao He(何宇昊), Chao-Lin Lü(吕超林), Li-Xing You(尤立星), Zhao-Hui Li(李召辉), Guang Wu(吴光), Wei-Jun Zhang(张伟君), Lu Zhang(张露), Xiao-Yu Liu(刘晓宇), Xiao-Yan Yang(杨晓燕), Zhen Wang(王镇)

Chin. Phys. B . 2018, 27(1): 018501. **doi:** 10.1088/1674-1056/27/1/018501

Photodetectors based on junctions of two-dimensional transition metal dichalcogenides

Xia Wei(魏侠), Fa-Guang Yan(闫法光), Chao Shen(申超), Quan-Shan Lv(吕全山), Kai-You Wang(王开友)

Chin. Phys. B . 2017, 26(3): 038504. **doi:** 10.1088/1674-1056/26/3/038504

High-speed waveguide-integrated Ge/Si avalanche photodetector

Hui Cong(丛慧), Chunlai Xue(薛春来), Zhi Liu(刘智), Chuanbo Li(李传波), Buwen Cheng(步成文), Qiming Wang(王启明)

Chin. Phys. B . 2016, 25(5): 058503. **doi:** 10.1088/1674-1056/25/5/058503

Design and fabrication of multi-channel photodetector array monolithic with arrayed waveguide grating

Qian-Qian Lv(吕倩倩), Pan Pan(潘盼), Han Ye(叶焓), Dong-Dong Yin(尹冬冬),Yu-Bing Wang(王玉冰), Xiao-Hong Yang(杨晓红), Qin Han(韩勤)

Chin. Phys. B . 2016, 25(3): 038505. **doi:** 10.1088/1674-1056/25/3/038505

TOPICAL REVIEW — Photodetector: Materials, physics, and applications

Review of deep ultraviolet photodetector based on gallium oxide*

Yuan Qin(覃愿)[1,3], Shibing Long(龙世兵)[2,3,†], Hang Dong(董航)[1,3], Qiming He(何启鸣)[1], Guangzhong Jian(菅光忠)[1,3], Ying Zhang(张颖)[1,3], Xiaohu Hou(侯小虎)[2], Pengju Tan(谭鹏举)[2], Zhongfang Zhang(张中方)[2], Hangbing Lv(吕杭炳)[1,3], Qi Liu(刘琦)[1,3], and Ming Liu(刘明)[1,3]

[1] *Key Laboratory of Microelectronics Devices & Integration Technology, Institute of Microelectronics, Chinese Academy of Sciences, Beijing* 100029, *China*
[2] *School of Microelectronics, University of Science and Technology of China, Hefei* 230026, *China*
[3] *University of Chinese Academy of Sciences, Beijing* 100049, *China*

(Received 17 September 2018; revised manuscript received 20 October 2018; published online 12 December 2018)

Ultraviolet (UV) photodetectors (PDs) have drawn great attention in recent years due to their potential application in civil and military fields. Because of its ultrawide bandgap, low cost, strong radiation hardness, and high thermal and chemical stability with high visible-light transparency, Ga_2O_3 is regarded as the most promising candidate for UV detection. Furthermore, the bandgap of Ga_2O_3 is as high as 4.7–4.9 eV, directly corresponding to the solar-blind UV detection band with wavelength less than 280 nm. There is no need of doping in Ga_2O_3 to tune its bandgap, compared to AlGaN, MgZnO, etc, thereby avoiding alloy composition fluctuations and phase separation. At present, solar-blind Ga_2O_3 photodetectors based on single crystal or amorphous Ga_2O_3 are mainly focused on metal–semiconductor–metal and Schottky photodiodes. In this work, the recent achievements of Ga_2O_3 photodetectors are systematically reviewed. The characteristics and performances of different photodetector structures based on single crystal Ga_2O_3 and amorphous Ga_2O_3 thin film are analyzed and compared. Finally, the prospects of Ga_2O_3 UV photodetectors are forecast.

Keywords: gallium oxide, ultrawide bandgap, ultraviolet (UV), photodetector

PACS: 85.60.Gz, 73.61.Ga **DOI:** 10.1088/1674-1056/28/1/018501

1. Introduction

Photodetectors (PD) are a key component in modern optoelectronic devices and are widely used in civil and military fields such as optical imaging, spatial optical communication, missile guidance and positioning navigation, and so on.[1–3] Currently, the main commercial UV photodetectors are Si-based photodiodes and photomultipliers due to the highly mature Si processes and their low cost.[4] However, because of its narrow bandgap (1.1–1.3 eV),[1–3] the detection band is limited from near UV to infrared light. Additionally, the Si based photodetector usually has a low efficiency and needs high vacuum conditions and high voltage (e.g., in photomultiplier).[5]

To avoid these disadvantages, UV photodetectors based on wide bandgap materials such as SiC, GaN, ZnO, Ga_2O_3, and diamond have gained more and more attention because of the intrinsic solar-blindness. Moreover, the wide bandgap semiconductors exhibit strong radiation hardness, high thermal and chemical stability, making them feasible to be applied in harsh environment.[6] What is more, GaN and ZnO can alloy with Al and MgO, respectively, to increase the bandgap to detect deeper UV light. However, the alloying process and relatively complicated growth technology will cause alloy composition fluctuations and phase separation, thereby introducing a large defect density and limiting its application under high demand conditions.[7]

Among wide bandgap materials, Ga_2O_3 has many unique characteristics, including high breakdown voltage and high Baliga's figure of merit (BFOM). These outstanding properties make Ga_2O_3 a promising material for high-temperature and high-power applications. In addition, its bandgap is 4.7–4.9 eV, which is intrinsically suitable for deep ultraviolet (DUV) photodetection[8] without any doping or alloying process. Besides, the growth cost of Ga_2O_3 is relatively low compared to other wide bandgap materials. The basic properties of Ga_2O_3 and other wide bandgap materials are listed in Table 1. The Ga_2O_3 photodetector was firstly reported by Takayoshi Oshima *et al.*[9] in 2007, and the research of Ga_2O_3 photodetector has flourished in recent years. In the beginning, the Ga_2O_3 photodetector was mainly based on the metal–semiconductor–metal (MSM) structure for its easy fabrication, and through improving the quality of Ga_2O_3, many solar-blind MSM Ga_2O_3 photodetectors with high performance were reported.[10,11] Gradually, other materials such as Si, ZnO, GaN, diamond and two-dimensional materials were used to form heterojunction with Ga_2O_3 to make Schottky photodiodes.[12–15] Key figures of merit are used to evaluate these photodetectors, as summarized in Table 2.

*Project supported by the National Natural Science Foundation of China (Grant Nos. 61521064, 61522408, 61574169, 61334007, 61474136, and 61574166), the Ministry of Science and Technology of China (Grant Nos. 2018YFB0406504, 2016YFA0201803, 2016YFA0203800, and 2017YFB0405603), the Key Research Program of Frontier Sciences of Chinese Academy of Sciences (Grant Nos. QYZDB-SSW-JSC048 and QYZDY-SSW-JSC001), and the Beijing Municipal Science and Technology Project, China (Grant No. Z171100002017011).

†Corresponding author. E-mail: shibinglong@ustc.edu.cn

© 2019 Chinese Physical Society and IOP Publishing Ltd http://iopscience.iop.org/cpbIOP161ZIOP161Z http://cpb.iphy.ac.cn

Table 1. The basic properties of Si and wide bandgap materials.

Materials	Si	MgZnO	4H–SiC	GaN	Diamond	β-Ga_2O_3
E_g/eV	1.1	3.7–7.8	3.3	3.4	5.5	4.8
μ/cm^2·V^{-1}·s^{-1}	1400	250	1000	1200	2000	300
E_{br}/MV·cm^{-1}	0.3	–	2.5	3.3	10	8
ε	11.8	4.6	9.7	9.0	5.5	10
BFOM ($\varepsilon\mu E_{br}^3$)	1	–	340	870	24664	3444
Thermal Conductivity/W·cm^{-1}·K^{-1}	1.5	1.2	2.7	2.1	10	0.11
Conductive type	n/p	n/p	n/p	n/p	p	n
Response Spectrum/nm	400–1100	200–370	270–380	200–300	<225	<280

Table 2. Key figures of merit for photodetectors.

Figures-of-merit	Expression	Unit	Definition
Responsivity	$R = \frac{I_p - I_d}{P}$	A/W	I_p and I_d are photocurrent and dark current, respectively. P is the light power irradiated on the photodetector.
External quantum efficiency	EQE $= \frac{hc}{e\lambda}R$	–	The number of photogenerated electrons per second divided by the number of incident photons on the device per second. Here h is the Planck constant, c is the speed of light, λ is the wavelength of the incident light, and e is the elementary electric charge.
Response time	τ_r, τ_d	s	The rise/decay time is defined as the time for the photocurrent to increase/decay from 10/90% to 90/10%.
Detectivity	$D = \sqrt{\frac{S}{2eI_d}}R$	Jones	The signal-to-noise ratio when one watt of light power is incident on a detector of area 1 cm^2, and the noise is measured over a 1 Hz bandwidth. S is the effective area of the photodetector.
Gain	$G = \tau_l/\tau_t$, $\tau_t = \frac{L^2}{\mu V_{bias}}$	–	The number of photogenerated carriers collected by the electrodes divided by the absorbed photons. τ_l is the life time of photo generated carriers and τ_t is the carrier transit time. L is the channel length. μ is the mobility, and V_{bias} is the bias voltage.
Linear dynamic range	LDR $= 20\log I_p/I_d$	dB	I_p and I_d are photocurrent and dark current, respectively. This equation is for estimation for imaging application.

In this paper, we review the recent achievements of Ga_2O_3 photodetectors. We focus on Ga_2O_3 photodetectors based on single crystal and amorphous Ga_2O_3 with different device structures, by analyzing its performance and characteristics. We firstly review the recent progress of MSM structure-based Ga_2O_3 photodetectors. Secondly, the Ga_2O_3 photodetectors based on Schottky junction are discussed. Finally, we give an outlook on the future direction in the field of Ga_2O_3 based UV photodetector.

2. MSM photodetectors

MSM Ga_2O_3 photodetectors were firstly proposed because of their fundamental advantages: (i) simple structure; (ii) easy fabrication and integration; and (iii) low capacitance per unit area. Usually, an MSM photodetector is composed of two back-to-back Schottky junctions by depositing interdigitated metal electrodes on the surface of the active layer. A schematic of MSM photodetector structure is shown in Fig. 1. The MSM photodetector usually has fast response speed because its low capacitance per unit area and low built-in electric field in the Schottky junction. The width and spacing of the interdigitated metal electrodes have great impact on the performance of the MSM photodetector. The drawback of MSM structure is its low responsivity due to the small active light absorbing area because of metallization for the electrodes. The performance of MSM Ga_2O_3 photodetectors is dependent on the quality of the materials, the substrate, the electrode structures, the doping of the Ga_2O_3 material, and the surface polariton of the Ga_2O_3 film. In this section, the influence of these factors on the performance of MSM Ga_2O_3 photodetectors is illustrated.

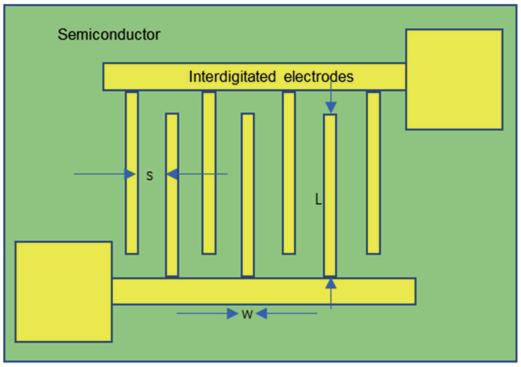


Fig. 1. Schematic structure of MSM photodetector.

It is well known that the performance of solar-blind photodetectors is strongly affected by the crystalline quality of the

Ga_2O_3 film. Different kinds of methods have been employed to grow Ga_2O_3 films, such as metal-organic chemical vapor deposition (MOCVD), molecular beam epitaxy (MBE), pulsed laser deposition (PLD), and magnetron sputtering.

Takayoshi Oshima *et al.*[9] first reported MSM Ga_2O_3 photodetectors in 2007, which were fabricated by a depositing β-Ga_2O_3 thin film on the *c*-plane sapphire substrates through molecular beam epitaxy. Ti/Au (50 nm/100 nm) were deposited to form ohmic contact electrodes in the metal–semiconductor–metal DUV photodetector. A small dark current of 1.2 nA at a bias voltage of 10 V was obtained (Figs. 2(a) and 2(b)). When the device was illuminated with 254 nm light, the current obviously increased. The photoresponsivity was 0.037 A/W, which corresponds to a quantum efficiency (QE) of 18%. After that, Anamika Singh Pratiyush *et al.*[16] used molecular beam epitaxy technology to grow β-Ga_2O_3 thin film on sapphire and fabricated an MSM photodetector (Figs. 2(c)–2(f)). Ni/Au with thicknesses of 20 nm/70 nm were deposited to form the Schottky contact. In their work, the researchers found that the photo current at 20 V was higher during the transient measurement compared to that in steady-state *I*–*V*. They attributed this phenomenon to the temporal dependence of photo-current due to possible trapping–detrapping transients. After the device was passivated with a 20 nm atomic layer deposited (ALD) Al_2O_3 at 250 °C, the effect was eliminated, indicating that the surface related traps are responsible for this effect. Usually, passivation with high *k* dielectric, rapid thermal annealing, surface treatment before metal contact deposition are beneficial to decrease the dark current, decrease the response and decay time, improve the responsivity, and hence enhance the overall performance of the MSM photodetector based on MBE grown β-Ga_2O_3 thin film. The MSM photodetector in this work presented high responsivity (> 1.5 A/W) at 4 V with low dark current at 20 V and high visible rejection ratio ($> 10^5$). What is more, the device showed fast response and decay speed without any persistent photoconductivity (PPC) effect, suggesting the high crystalline quality of the MBE grown β-Ga_2O_3 thin film.

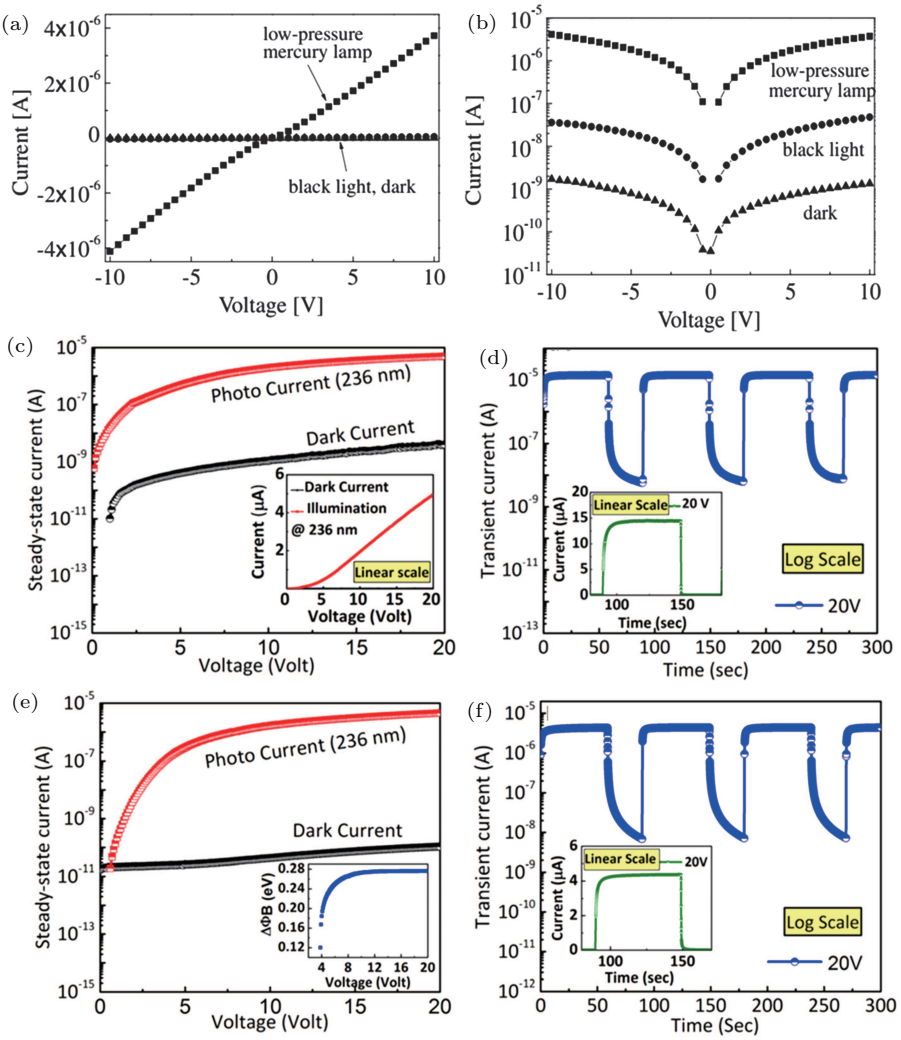


Fig. 2. (a) and (b) Linear and log scale current–voltage characteristics of the Ti/Au/β-Ga_2O_3 MSM DUV photodetector in the dark, under black light irradiation, and under low-pressure mercury lamp irradiation.[9] (c) Steady-state *I*–*V* characteristic under light illumination and *I*–*V* characteristics in the dark (log scale), and (d) the time-dependent photoresponse under the illumination of 236 nm at 20 V (log scale) of the Ni/Au/β-Ga_2O_3 MSM photodetector before Al_2O_3 passivation. (e) *I*–*V* characteristic under light illumination and *I*–*V* characteristics in the dark (log scale), and (f) time-dependent photoresponse under the illumination of 236 nm at 20 V (log scale) of the Ni/Au/β-Ga_2O_3 MSM photodetector after Al_2O_3 passivation.[16]

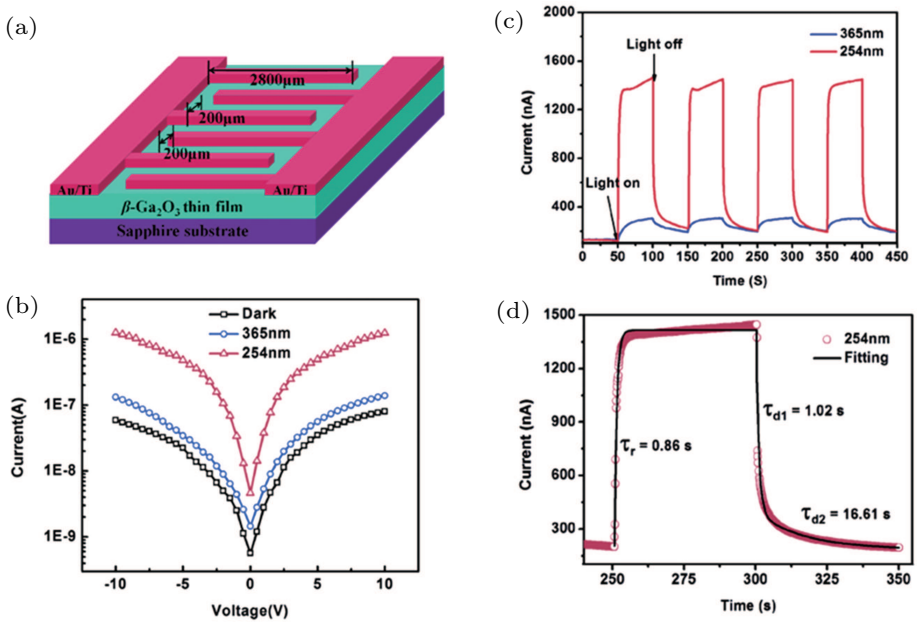


Fig. 3. (a) Schematic diagram of the fabricated Ti/Au/β-Ga_2O_3 thin film MSM structure photodetector. (b) *I–V* characteristics of the Ti/Au/β-Ga_2O_3 photodetector in dark, under 365 nm light and under 254 nm light illumination in a logarithmic coordinate. (c) Time-dependent photoresponse of the Ti/Au/β-Ga_2O_3 photodetector under UV light illumination at bias voltage of 10 V. (d) Experimental current rise and decay process of the photodetector under 254 nm illumination (red hollow points) and its corresponding fitting curve (black solid line).[17]

On the other hand, Weihua Tang *et al.*[17] reported β-Ga_2O_3 thin film based solar-blind photodetector by LMBE technology. By optimizing the growth parameters, $(\bar{2}01)$ oriented β-Ga_2O_3 thin film deposited on sapphire substrate was obtained. Ultraviolet–visible absorption spectrum demonstrated that the prepared β-Ga_2O_3 thin film showed excellent solar-blind ultraviolet (UV) characteristics with a band gap of 5.02 eV. Ti/Au was deposited to form the interdigital metal electrodes, and subsequently thermal annealing was conducted at 300 °C for 10 min in Ar atmosphere. In Fig. 3, it can be seen that the dark current is approximately 128 nA, and the photocurrent of 1460 nA under 254 nm illumination is more than one order of magnitude larger than the dark current. According to the time-dependent photoresponse of the detector to 365 nm and 254 nm illumination by on/off switching under an applied bias of 10 V and a fitting with a biexponential relaxation equation, the rise time was 0.86 s, and the decay process consisted of two components with a fast-response component (1.02 s) and a slow-response component (16.61 s). They proposed that the time constant of the transient decay was governed by the depth of these traps and can be very long. The presence of numerous trapping states prevents carriers' recombination, which might cause the slow recovery time. It can be suggested that the poor quality of the β-Ga_2O_3 film strongly limits the performance of MSM β-Ga_2O_3 photodetectors.

In order to improve the response and recovery speed, Weihua Tang's group *in situ* annealed the thin film deposited by LMBE under an oxygen pressure of 100 Pa at 800 °C for 2 h.[18] They found that the Au/Ti electrodes were ohmic contact with the as-grown films and Schottky contact with the annealed films. The Schottky-type β-Ga_2O_3 photodetector exhibited lower dark current, higher responsivity, and shorter switching time. From the *I–V* characteristics (Fig. 4(a)), it can be seen obviously that the Ti/Au electrode was Schottky contact with the Ga_2O_3 thin film. The Schottky-type Ga_2O_3 photodetector are faster than the ohmic-type Ga_2O_3 photodetector in the response speed and recovery speed (Figs. 4(c) and 4(d)). By comparing the O 1s XPS spectra of the as-grown and post-annealed Ga_2O_3 thin films (Fig. 4(b)), it can be found that the oxygen vacancy concentration decreased in the post-annealed Ga_2O_3 thin films. The high performance of the Schottky-type Ga_2O_3 photodetector under 254 nm illumination greatly benefits from the Schottky barrier-controlled electron transport and the significant improvement of the quality of the β-Ga_2O_3 film, thus decreasing the quantity of photogenerated carriers trapped by oxygen vacancy.

Chiungyi Huang *et al.*[19] employed MOCVD to grow single-crystalline β-Ga_2O_3 film on (0001) sapphire substrate at low temperature and low pressure environment. The MSM β-Ga_2O_3 solar-blind photodetector was fabricated. The as-grown β-Ga_2O_3 film was annealed at 800 °C in atmosphere or in a nitrogen environment, and the thermal annealing effect on the material characteristics of β-Ga_2O_3 film was investigated. Through x-ray diffraction (XRD), cathodoluminescence (CL) measurement, and *I–V* characterization of the MSM β-Ga_2O_3 solar-blind photodetector, they concluded that the film annealed at 800 °C for 15 min in a nitrogen atmosphere would result in improved material characteristics and enhanced device performance. After annealing, the device exhibited lower dark current, which suggested the improved crystalline qual-

ity of the β-Ga_2O_3 epilayer. Besides, Dezhen Shen *et al.*[20] reported their fabrication of MSM β-Ga_2O_3 solar-blind photodetector on sapphire substrate based on MOCVD deposited β-Ga_2O_3 film. Au was deposited as the interdigital electrodes. The fabricated photodetectors exhibited a high responsivity of 17 A/W, UV-to-dark rejection ratio of 8.5×10^6, and EQE of 8228% at 20 V due to the carrier multiplication occurred in the Ga_2O_3 under Au electrodes.

The crystalline quality of β-Ga_2O_3 film is readily affected by various factors, one of which is the thermal-expansion or lattice match with the substrate. Qian Feng *et al.*[21] made a comparison study of the performance of the β-Ga_2O_3 photodetectors on bulk β-Ga_2O_3 substrate and sapphire. LMBE technology was used to grow epitaxial film on bulk β-Ga_2O_3 substrate and *c*-sapphire substrate. Ti/Au with 10 nm/40 nm thickness was used as the interdigital Schottky contacts. The schematic of the Ga_2O_3 photodetector is shown in Figs. 5(a) and 5(b). Material characterization was conducted to characterize the quality of the epitaxial thin film on bulk β-Ga_2O_3 substrate and *c*-sapphire substrate (Figs. 5(c)–5(f)). The high resolution transmission electron microscope (HRTEM) image indicates the epitaxial film on bulk β-Ga_2O_3 substrate has high crystal quality and smooth surface. Figure 5(d) shows the XRD curves of the epitaxial film and the results indicate that both films are β phase. It also can be found that the peaks of Ga_2O_3 on sapphire move to the low-angle side with different degrees of shift, suggesting that there is an out-of-plane tensile strain in the Ga_2O_3 film on the sapphire substrate. Furthermore, the atomic force microscope (AFM) results indicate that the epitaxial film on the bulk β-Ga_2O_3 has a much smoother surface (Figs. 5(e) and 5(f)). All results suggest that the epitaxial film on the bulk β-Ga_2O_3 has a higher crystal quality.

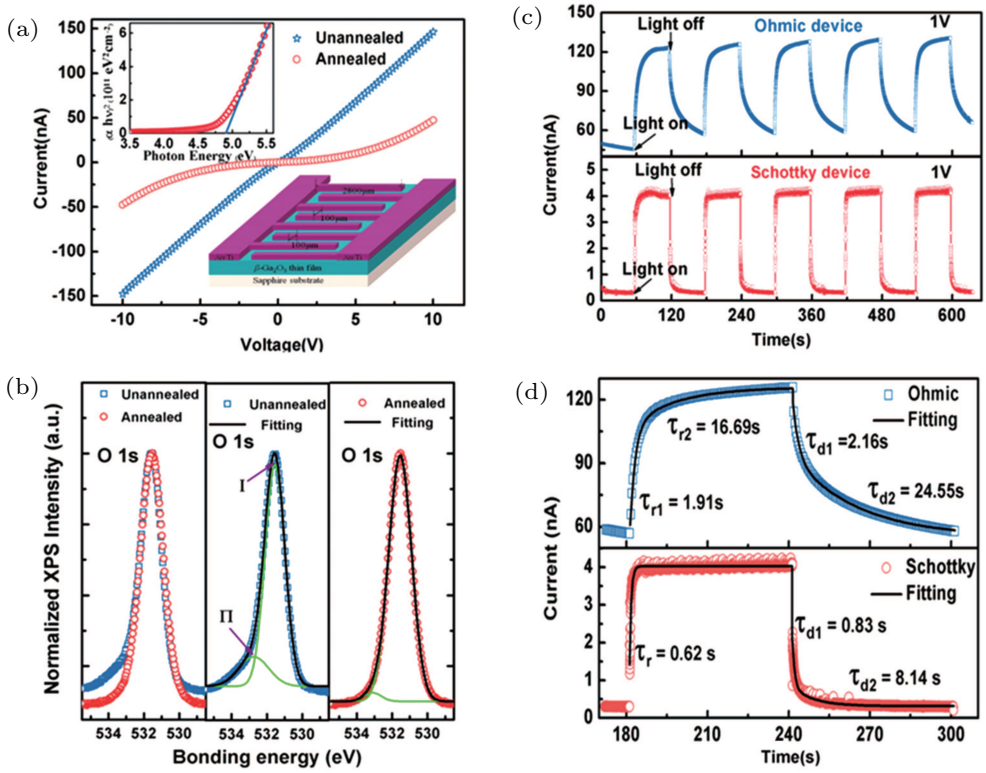


Fig. 4. (a) The *I*–*V* characteristics of the β-Ga_2O_3 thin films MSM photodetector without and with annealing treatment in O_2 atmosphere in the dark. The inset (bottom right) shows the schematic figure of the MSM structure. The inset (top left) is the plot of $(\alpha h\nu)^2$ as a function of $h\nu$ calculating from UV–vis absorbance spectrum of the β-Ga_2O_3 thin film. (b) Normalized O 1s XPS spectra of the as-grown and post-annealed β-Ga_2O_3 thin films. (c) Time-dependent photoresponse of the β-Ga_2O_3 thin films MSM photodetector under 254 nm illumination. (d) Enlarged view of the rise/decay edges of the transient photoresponse curve and its corresponding exponential fitting.[18]

The optical-electrical characteristics of the above photodetectors are presented in Fig. 6. The bulk Ga_2O_3 device showed lower dark current and higher photocurrent, consequently, an improved photo to dark current ratio (PDCR) was achieved. In Figs. 6(c) and 6(d), it can be obviously found that the bulk Ga_2O_3 photodetector presents a remarkably enhanced responsivity over the device on sapphire in a wide range of ultraviolet wavelength. Besides, a blueshift in responsivity can be observed in the Ga_2O_3 photodetector on sapphire compared with that on bulk Ga_2O_3 substrate. The cutoff wavelength is 253 nm, indicating that bandgap E_g of the epitaxial Ga_2O_3 on sapphire is 4.90 eV. This change of bandgap is induced by strain in semiconductor. The time-dependent photoresponse characteristics of the devices were measured under 254 nm light with an intensity of 38 $\mu W/cm^2$ and a bias voltage of 20 V. The response and decay processes can be both divided

into fast and slow durations. The fast response is directly related to the inter-band optical transition. The slow-response in the rise process might be resulted from the optical absorption between band edges and some defect bands. The slower decay process is dominated by the releasing of the captured carriers by some trapping states, which leads to a more pronounced persistent photoconductivity (PPC) caused by oxygen vacancies. In Fig. 6(e), we can see that the τ_{d2} of bulk Ga_2O_3 device is smaller than that of Ga_2O_3 device on sapphire, indicating that there is less density of oxygen vacancies in the epitaxial film on bulk Ga_2O_3 in comparison with the material epitaxially grown on sapphire. In conclusion, the higher crystal quality in bulk Ga_2O_3 device leads to the significantly enhanced photocurrent, dark current, PDCR, and responsivity performance.

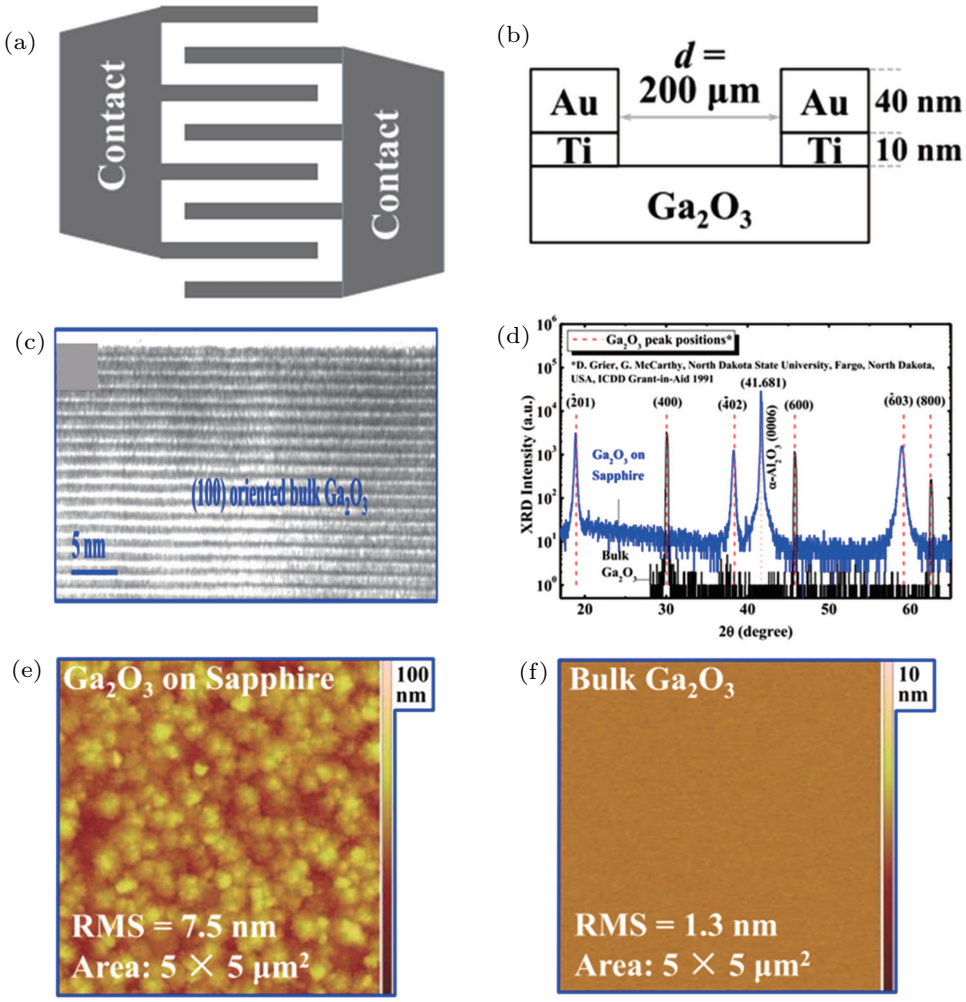


Fig. 5. (a) Top view and (b) cross-sectional schematics of the Ti/Au/Ga_2O_3 MSM Ga_2O_3 photodetector. (c) HRTEM image of Ga_2O_3 grown on bulk Ga_2O_3 substrate. (d) XRD curves for Ga_2O_3 device samples on sapphire and bulk. AFM images of (e) Ga_2O_3 grown on sapphire and (f) bulk Ga_2O_3.[21]

To the best of our knowledge, almost all the reported MSM β-Ga_2O_3 photodetectors were based on sapphire substrate. However, there was no report of MSM β-Ga_2O_3 photodetectors on the cost-effective Si substrate due to its large lattice and thermal expansion coefficient mismatch with β-Ga_2O_3. Until recently, Kanika Arora *et al.*[10] reported an ultrahigh performance of self-powered β-Ga_2O_3 thin film solar-blind photodetector on Si substrate through magnetron sputtering method. By using high temperature seed layer (HSL), the improved crystalline quality was achieved in comparison to the Ga_2O_3 thin film grown without a high-temperature seed layer. The device exhibited a high on/off ($I_{254\ nm}/I_{dark}$) ratio of $> 10^3$, a record-low dark current of 1.43 pA, and high stability and reproducibility over 100 cycles even after 2100 h at zero bias. What is more, the photodetector yielded a responsivity as high as 96.13 A/W, with an external quantum efficiency of 4.76×10^4 at 5 V under light illumination of 250 nm. Figures 7(a) and 7(b) show the schematic of the fabrication processes and temperature profile for the growth of a high temperature seed-layer-assisted β-Ga_2O_3 thin film. Annealing steps and growth are mixed to reduce the thermal expansion mismatch between Ga_2O_3 and Si substrate. From Fig. 7(c), it can be seen clearly that the sample deposited without HSL has a sharp increase of the dark current with bias, which is due to the existence of high concentration defect states. It also can be observed that the photocurrent of the sample deposited with HSL increases significantly under 250 nm light illumination, thus leading to a higher photo-to-dark current ratio.

The sample deposited with HSL exhibits higher responsivity and EQE due to the high internal gain, which is associated with shallow traps populated at the metal–semiconductor interface. These traps will capture the photogenerated holes and prevent the recombination of the electrons under DUV illumination and substantially contribute to a significant photocurrent. Figure 7(e) presents the time-dependent photoresponse with HSL assisted β-Ga_2O_3 thin film photodetector. It can be obviously found that the device has extremely low dark current and high response speed, which was reported to be associated with the charge carrier mobility, electron–hole lifetime, and efficient charge separation in the interface between Au and β-Ga_2O_3 thin film. This work provides new guidelines to fabricate MSM β-Ga_2O_3 thin film photodetector with ultrahigh performance using cost-effective magnetron sputtering on Si substrate.

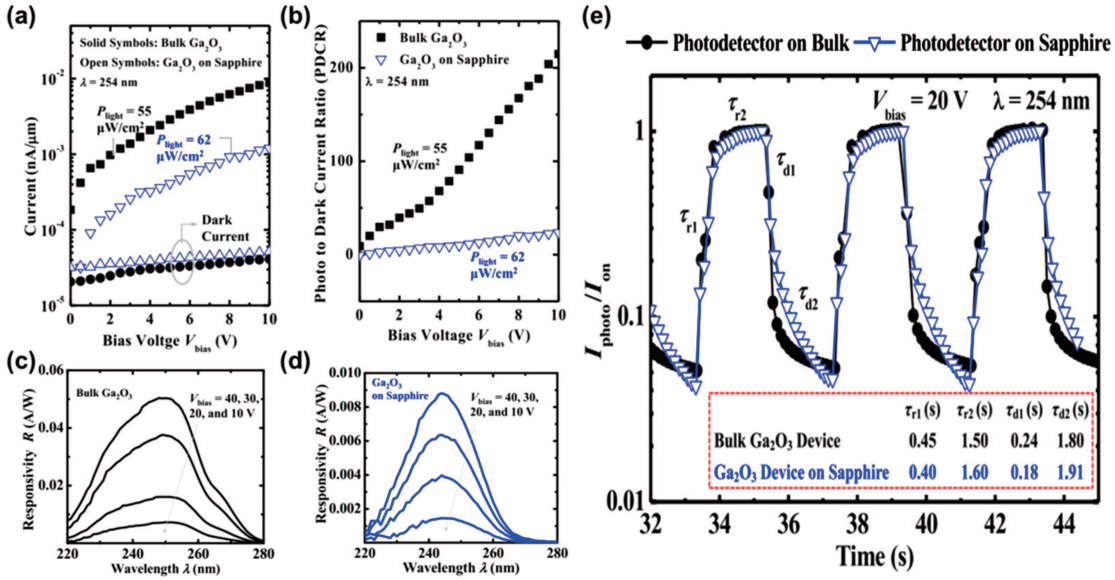


Fig. 6. (a) *I–V* characteristics for the MSM photodetectors on bulk Ga_2O_3 and sapphire in the dark and under light illumination of 254 nm. (b) PDCR for devices on bulk Ga_2O_3 and sapphire. Responsivity as a function of illumination optical wavelength λ for the Ga_2O_3 MSM photodetectors on (c) bulk Ga_2O_3 and (d) sapphire substrate at various V_{bias}, respectively. (e) Time-dependent photoresponse of the MSM photodetectors on bulk Ga_2O_3 and on sapphire under a bias voltage of 20 V. The inset lists the response and decay time of the devices.[21]

Recently, more and more works were reported in the fabrication of MSM GaO_x photodetectors based on the cost-effective radio frequency (RF) magnetron sputtered GaO_x film instead of expensive MOCVD, MBE, or LMBE technology. Among them, some photodetectors exhibited surprisingly high performances, even exceeding those of the majority of Ga_2O_3 photodetectors based on β-Ga_2O_3 thin film deposited by MOCVD, MBE, or LMBE technology. Ling-Xuan Qian *et al.*[11] demonstrated an ultrahigh responsivity and rapid recovery MSM photodetector based on magnetron sputtered amorphous gallium oxide thin film. Another MSM photodetector based on β-Ga_2O_3 thin film deposited by MBE was fabricated as the control sample. Ti/Al was used as the interdigital electrodes. It can be found that the MBE deposited film was single crystal β phase Ga_2O_3, and the magnetron sputtering deposited sample was amorphous Ga_2O_3 (Fig. 8(a)). Figures 8(b) and 8(c) show the three-dimensional AFM surface images of the MBE and magnetron sputtering films. A larger RMS surface roughness value of 2.102 nm was found in the magnetron sputtering film, indicating that more surface defect states might generate during the sputtering process. In order to further characterize the material, XPS was conducted to measure the concentration of oxygen vacancies in the film (Fig. 8(d)). Obviously, the sputtering-deposited film contained more than twice oxygen vacancies than the MBE-grown one. The Ti/Al was confirmed to be Schottky contact and ohmic contact for the MBE-grown and magnetron sputtering deposited films, respectively (Fig. 9(b)), in consequence of which, the dark current of the MSM photodetector based on the magnetron sputtering film was larger than that of the MBE-grown one. Under DUV light illumination (254 nm), the magnetron sputtering-deposited photodetector exhibited higher photocurrent. The origin of the ohmic contact is probably associated the high concentration oxygen vacancies and other defect states in the magnetron sputtered gallium oxide thin film, which can lower the effective barrier height at the metal/a-GaO_x interface relative to that of the metal/β-Ga_2O_3 interface and facilitate the direct tunneling of electrons at the reverse-biased Schottky barrier. And the deep-level trap states may act as efficient trapping states and promote trap-assisted tunneling. The MSM photodetectors based on magnetron sputtering thin film exhibited a high responsivity of 70.26 A/W due to a high internal gain and the contribution of extrinsic transitions. What is more, the device showed a high 250 nm/350 nm rejection ratio exceeding 10^5, a high detectivity of 1.26×10^{14} Jones, and a rapid recovery (0.10 s) without any PPC effect which was attributed to effective surface recombination. This work made a comprehensive study of the

MSM photodetectors based on magnetron-sputtered film and revealed a pathway for the development of cost-effective, high performance solar-blind photodetectors.

Shujuan Cui *et al.*[22] also fabricated an amorphous Ga_2O_3 solar-blind photodetector with high response speed (19.1 μs) on rigid (quartz) and flexible polyethylene naphthalate (PEN) substrates by magnetron sputtering. Comprehensive study of the effect of oxygen flux in the sputtering process was conducted to reveal the origin of the high response speed of the MSM Ga_2O_3 solar-blind photodetector. The indium tin oxide (ITO) was used to act as the interdigital electrodes and can form good Schottky contact on amorphous Ga_2O_3 surface. With increasing oxygen flux in the sputtering process, the dark current was observed to decrease. Correspondingly, the photocurrent was smaller when the oxygen flux was larger. The researchers extracted the heights of the Schottky barrier and found that the Schottky barrier height increased with the increasing oxygen flux in the sputtering process. All the samples sputtered with O_2 incorporated (S1–S4) had relatively asymmetric barriers compared to the pure Ar sputtered sample (S0), indicating the existence of negative surface states. All the samples show a good stability and reproducibility and it is effective to improve the response speed by delicately increasing the oxygen flux. Only the pure Ar sputtered sample (S0) has a severe PPC phenomenon due to the existence of large amounts of oxygen vacancies. After introducing trace amount of oxygen during the sputtering process, the PPC effect can be significantly suppressed, and the response and decay speed are greatly improved. According to the XPS measurement, the Ga $2p_{3/2}$ peak is observed to move from 1117.6 eV to 1119.8 eV when increasing the oxygen flux from 0 to 0.15 sccm. Such a big shift suggests a more adequate oxidation state for gallium atoms in a-Ga_2O_3. What is more, the area ratios of the

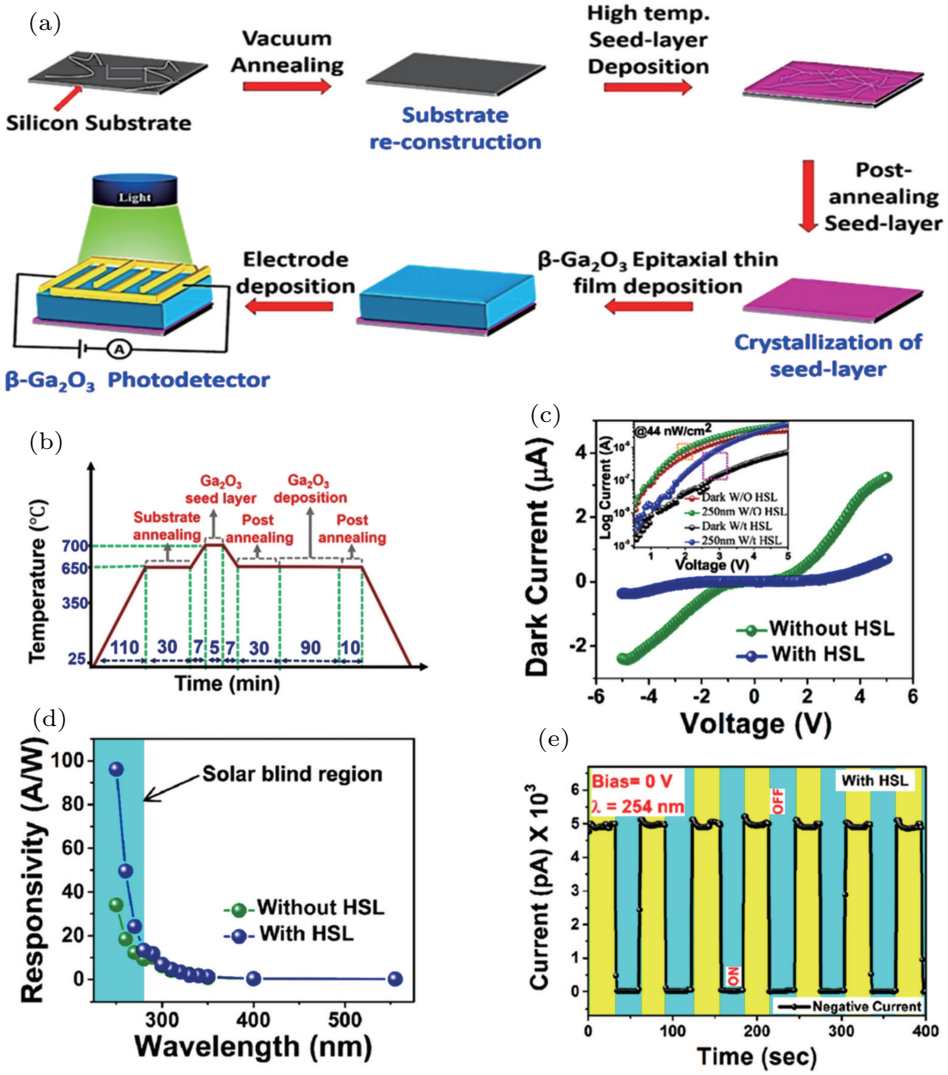


Fig. 7. (a) Schematic representation of the fabrication processes of MSM β-Ga_2O_3 solar-blind photodetectors. (b) Temperature profile for the growth process of the seed-layer-assisted β-Ga_2O_3 thin film. (c) *I*–*V* characteristics of MSM β-Ga_2O_3 solar-blind photodetectors based on thin films deposited without and with HSL conditions in the dark. Inset shows the *I*–*V* curves of MSM β-Ga_2O_3 solar-blind photodetectors without and with HSL conditions at 250 nm and in the dark in a semilogarithmic coordinate. (d) Photoresponsivity as a function of wavelength of the MSM β-Ga_2O_3 solar-blind photodetectors grown without and with HSL conditions. (e) Time-dependent photoresponse of MSM β-Ga_2O_3 solar-blind photodetectors deposited without and with HSL, respectively.[10]

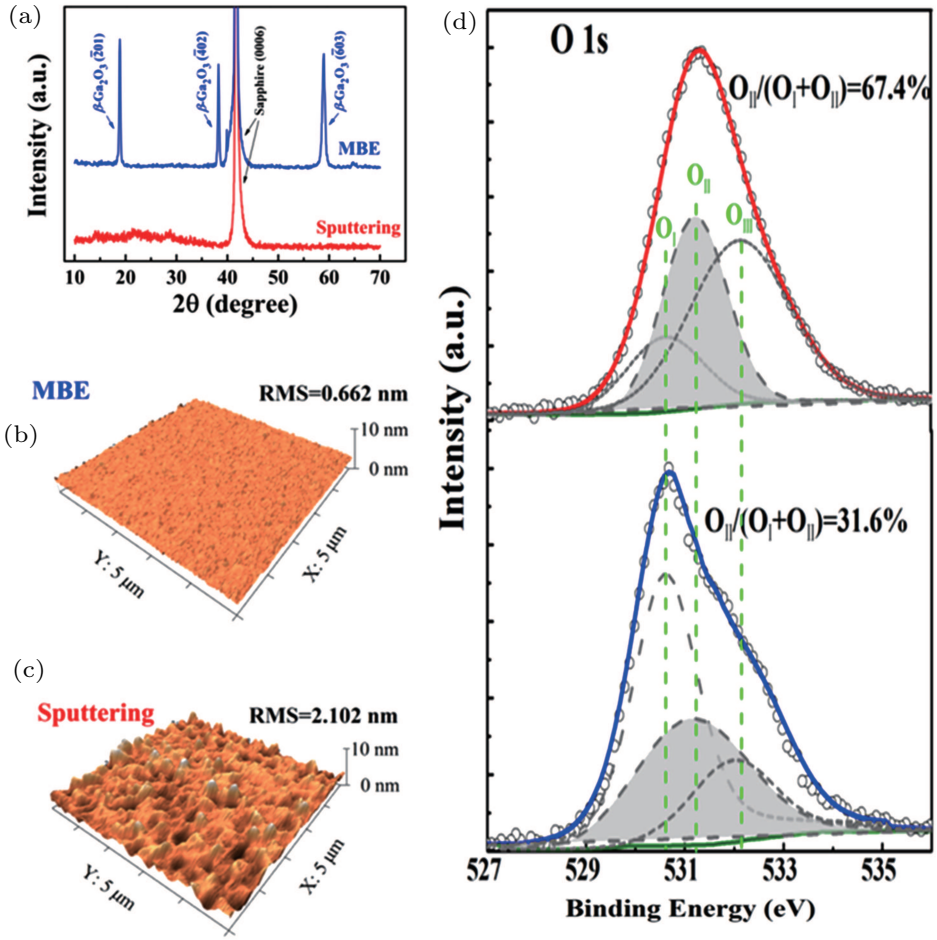


Fig. 8. (a) XRD patterns and three-dimensional AFM surface images of the gallium oxide films deposited by (b) plasma-assisted MBE and (c) magnetron sputtering. (d) Normalized XPS O 1s core-level spectra of the gallium oxide films deposited by magnetron sputtering (red) and plasma-assisted MBE (blue), respectively.[11]

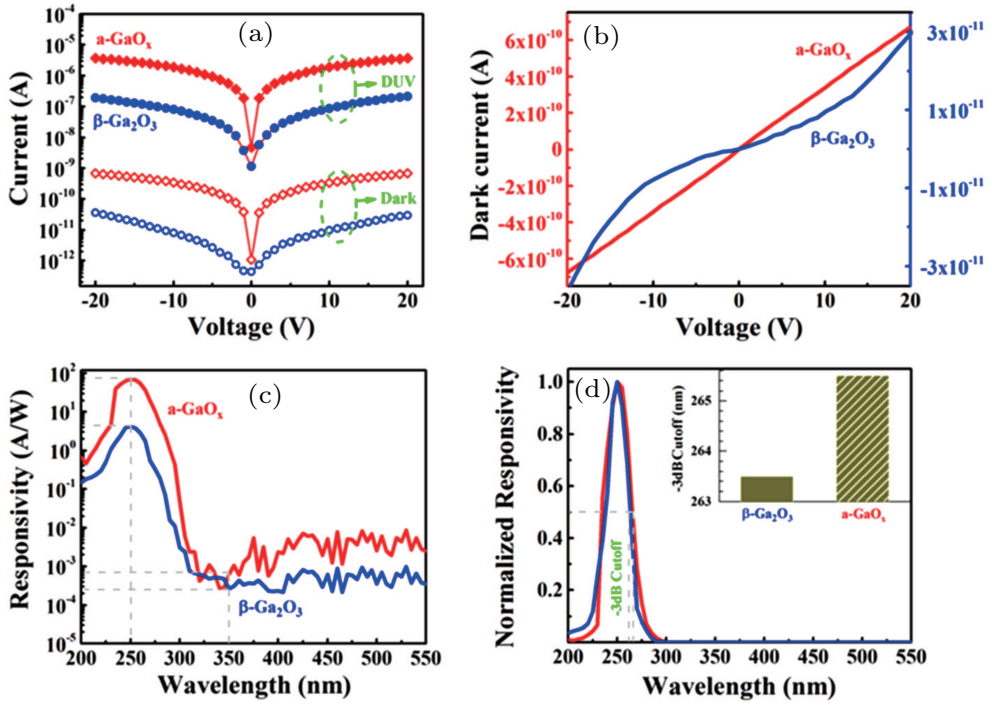


Fig. 9. (a) The *I–V* characteristics of the MSM gallium oxide photodetectors in the dark and under illumination of 254 nm light in a semilogarithmic coordinate. (b) Dark current of the photodetectors on a linear scale. (c) Responsivity vs. illumination optical wavelength on a semilogarithmic scale and (d) normalized spectral response of the MSM gallium oxide photodetectors based on a-GaO_x (red) and β-Ga_2O_3 (blue) thin films. The inset in (d) shows the cutoff wavelength of the photodetectors.[11]

O 1s and Ga 2p peaks (S_{O1s}/S_{Ga2p}) are 0.61, 0.64, and 0.65 for S0, S1, and S4, respectively. The increasing S_{O1s}/S_{Ga2p} shows an increase of oxygen content in the film and thus a reduction of oxygen vacancies. All the results suggest that the reduction of oxygen vacancies and the increase of Schottky barrier height can significantly promote the response speed. Besides, no obvious degradation of the photoelectric performance in bending states and fatigue tests was observed on the flexible device, suggesting the stability and applicability of the amorphous Ga_2O_3 thin film in the flexible solar-blind photodetectors. These results indicate that RF-magnetron sputtering can be employed to deposit Ga_2O_x film on various substrates and high performance MSM photodetectors can be achieved.

Si p–i–n diode with high performance is a common commercial photodetector. For the practical application of Ga_2O_3 p–i–n diode, p-type β-Ga_2O_3 thin film is essential. However, the achievement of p-type β-Ga_2O_3 thin film still remains a challenge because of lacking of suitable dopants, just like other oxide semiconductors, overcompensated by oxygen vacancy.[23,24] Weihua Tang *et al.*[25] tried to dope Mg into β-Ga_2O_3 thin film, and a weak p-type β-Ga_2O_3 thin film was obtained by RF magnetron sputtering for the first time. The Mg-doped β-Ga_2O_3 thin film was used to fabricate the MSM solar-blind photodetector. The as-fabricated photodetector exhibited a lower dark current, a higher sensitivity, and a relatively faster decay time. This is probably due to the high insulativity and low defect concentration in the p-type Mg-doped Ga_2O_3 thin film. This work suggests that doping other elements into Ga_2O_3 thin film might be a new way for the development of Ga_2O_3 solar-blind photodetector with high performance in the future.

Almost at the same time, Fikadu Alema *et al.*[23] reported the fabrication and characterization of MSM solar-blind photodetector based on Zn doped β-Ga_2O_3 epitaxial thin film. The epitaxial ZnGaO thin film was grown on *c*-sapphire substrate by MOCVD technology. High responsivity $> 10^3$ A/W was achieved due to the existence of a large amount of defect states in the as-grown film with enhanced internal gain. By post-annealing, the quality of the epitaxial thin film was well improved and the dark current was reduced from nA to pA, as shown in Fig. 6, and consequently an increased rejection ratio $R_{232\ nm}/R_{320\ nm}$. At a bias voltage of 20 V, the responsivity and rejection ratio were calculated to be 210 A/W (232 nm) and 5×10^4, respectively. However, these parameters of the β-Ga_2O_3 thin film based MSM photodetector were found to be much smaller, suggesting that the ZnGaO solar-blind photodetector has superior performance and is a potential candidate for future applications.

Qian Feng *et al.*[26] tried to dope Al into the β-Ga_2O_3 film and the single crystallinity $(AlGa)_2O_3$ epitaxial film was obtained on sapphire substrate. The $(AlGa)_2O_3$ epitaxial film exhibited wider bandgap compared to β-Ga_2O_3. The $(AlGa)_2O_3$ solar-blind photodetector showed higher photocurrent and enhanced responsivity, which was due to the enhanced conductivity of the material caused by shallow defects in the $(AlGa)_2O_3$ epitaxial film. However, when the Al composition increased up to a specific value, significant performance degradation of the $(AlGa)_2O_3$ solar-blind photodetector was observed, which was probably associated with the deep defects. It can be concluded that suitable dopants can modify the material characteristics: change the bandgap, improve the crystalline quality and electrical characteristics, and so on. Doping with optimized composition is a good way to fabricate high performance solar-blind Ga_2O_3 photodetectors in the future. Recently, Shuo-Huang Yuan *et al.*[27] reported an MSM aluminum–gallium oxide (AGO) photodetector with improved responsivity drop from 250 nm to 200 nm by incorporating trace aluminum into gallium oxide through magnetron sputtering. By optimizing the Al content, the dark current, photocurrent, responsivity, and detectivity of AGO PD were enhanced by 0.83, 46.4, 53.61, and 96.5 times, respectively, greater than those of the GO one. What is more, the solar-blind AGO photodetector based on magnetron sputtered AGO film showed higher performance than that deposited by MBE techonology,[26] which suggested that the magnetron sputtered AGO film has great potential for deep UV photodetection.

Surface plasmon polariton is an electro-magnetic wave coupled to free electron oscillations near the surface of metal, and has usually been used to improve the photoelectric properties in many optoelectronic devices. In order to enhance the performance of the Ga_2O_3 photodetector, Yuehua An *et al.*[28] introduced surface plasmon Au to form Au nanoparticles (NPs)/β-Ga_2O_3 composite thin film. The Au ultra-thin film was deposited on the β-Ga_2O_3 thin film followed by post-thermal treatment. The Au NPs/β-Ga_2O_3 composite thin film presents another significant absorption around 510 nm besides the absorption at the wavelength of less than 250 nm induced by the β-Ga_2O_3 thin film. The photoelectric performance of the Au NPs/β-Ga_2O_3 composite thin film-based photodetector is much higher than the pure β-Ga_2O_3 photodetector because of the assistance of surface plasmon polariton effect. Besides, Shujuan Cui *et al.*[29] reported a Ga/Ga_2O_3 nanocomposite solar-blind photodetector. Photoresponse enhancement was achieved by incorporating Ga surface plasmon into the nanocomposite film. By optimizing the thickness of the Ga interlayer, the Ga_2O_3/Ga/Ga_2O_3 photodetector exhibited an extremely low dark current of 8.52 pA at 10 V bias, a very high light-to-dark ratio of $\sim 8 \times 10^5$ and a responsivity of 2.85 A/W at 15 V bias. These results indicate that the plasmonics are important to improve the photoresponse characteristics of the Ga_2O_3 photodetector and the plasma modified Ga_2O_3 photodetector is a potential candidate for practical application.

There are a few reported works on the MSM photodetectors based on exfoliated β-Ga_2O_3 micro-flake.[30,31] Ni/Au was selected to form the Schottky contact and extremely low dark current and high sensitivity (ratio of photocurrent to dark current $> 10^3$) were obtained.[31] A fast switching speed of 0.53 s and responsivity of 1.68 A/W indicate the potential of the quasi-two-dimensional β-Ga_2O_3 for optoelectronic applications. Sooyeoun Oh *et al.*[30] reported a high responsivity exfoliated β-Ga_2O_3 MSM photodetector with graphene as the Schottky contact (Fig. 10(a)). In comparison, β-Ga_2O_3 MSM with Ni/Au as the Schottky contacts was fabricated. The β-Ga_2O_3 MSM photodetector with graphene electrodes exhibited much higher photoelectric performance than that with Ni/Au electrodes, including higher responsivity ($\sim$ 29.8 A/W), photo-to-dark current ratio ($\sim 1 \times 10^6$%), rejection ratio ($R_{254\ \mathrm{nm}}/R_{365\ \mathrm{nm}} \sim 9.4 \times 10^3$), detectivity ($\sim 1 \times 10^{12}$ Jones), and operating speed to 254 nm light. The β-Ga_2O_3 MSM photodetector with graphene electrodes has extremely low dark current due to the back-to-back Schottky barrier. Besides, because the graphene is transparent, the increased light absorption area under light illumination leads to more carriers generating below the transparent electrodes, as a consequence of which, the depletion region narrows, allowing the tunneling transport through the narrowed Schottky barrier. Thus, an enhanced photocurrent is obtained in the β-Ga_2O_3 MSM photodetector with graphene electrodes. The high performance of the β-Ga_2O_3 MSM photodetector with graphene electrodes is attributed to the low dark current resulting from the presence of a Schottky barrier under dark condition and the high photocurrent due to the tunneling effect under 254 nm illumination.

In recent years, solar-blind Ga_2O_3 photodetectors have achieved much progress and the high-performance photodetectors with high responsivity, high detectivity, and high response speed are approaching to practical application. For example, the solar-blind Ga_2O_3 photodetectors are a potential candidate for DUV imaging. However, the photodetector array is a prerequisite for real-time imaging and can also improve the detectivity sensitivity. Recently, Yangke Peng *et al.*[32] firstly fabricated the highly integrated MSM Ga_2O_3 32×32, 16×16, 8×8, and 4×4 photodetector arrays. The image of the photodetectors arrays and their microstructure are shown in Fig. 11. A 4-1 photodetector cell was chosen to demonstrate the performance of the photodetectors. The photodetectors exhibited a responsivity of 8.926×10^{-1} A/W under 250 nm light illumination at a 10 V bias voltage with fast rise time and decay time of 305 ms and 251 ms, respectively. All photodetector cells have a consistent responsivity with a standard deviation of 12.1%. This result renders the MSM Ga_2O_3 photodetector a promising building block for future imaging application. Table 3 summarizes the key figures of merit of MSM Ga_2O_3 photodetectors reported in recent years.

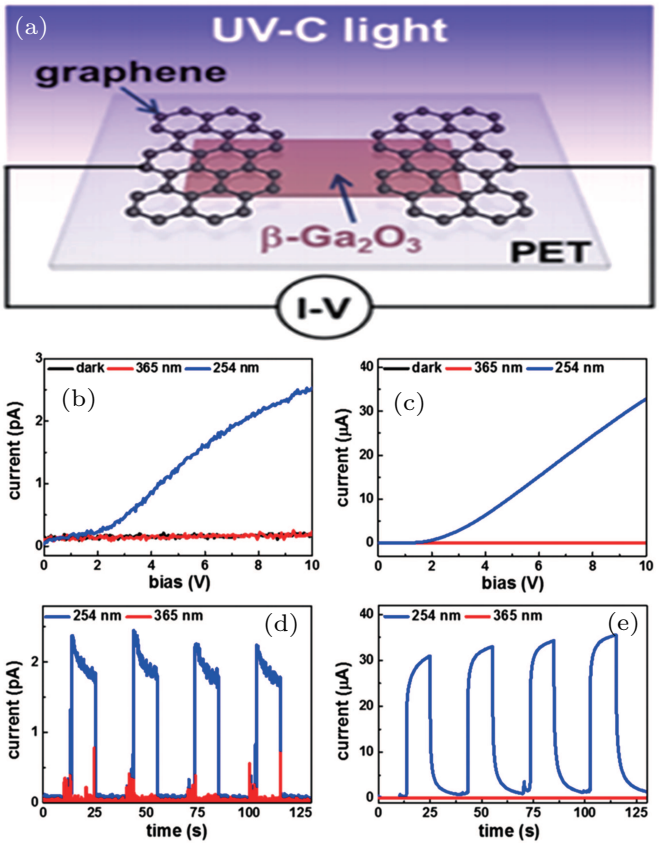


Fig. 10. (a) Schematic diagram of the exfoliated β-Ga_2O_3 flake based MSM solar-blind photodetector with graphene electrodes. *I–V* characteristics of the fabricated solar-blind MSM photodetectors in the dark and under light illumination at different conditions (254 nm or 365 nm): (b) with Ni/Au contacts and (c) with graphene contacts. Time-dependent photoresponse of the exfoliated β-Ga_2O_3 flake based MSM solar-blind photodetectors under 254 nm or 365 nm light illumination (d) with Ni/Au contacts and (e) with graphene contacts.[30]

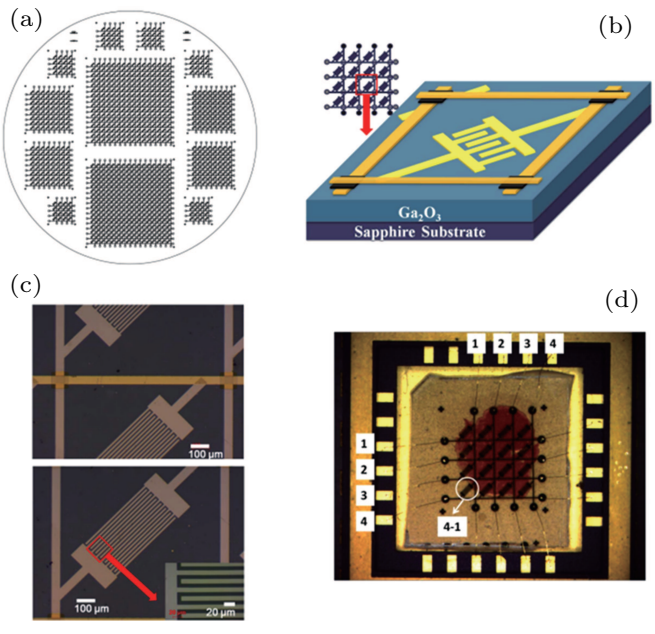


Fig. 11. (a) The image of photodetectors arrays. (b) Schematic diagram of the photodetectors arrays. (c) The microstructure image of the fabricated devices. (d) Photograph of the photodetectors arrays packaged in ceramic packages.[32]

Table 3. Comparison of key figures of merit of recent Ga_2O_3 based MSM photodetectors.

Materials and structures	Growth method	R/A·W^{-1}	τ_r/τ_d	D^*/Jones	EQE/%	Dark current	UV/dark rejection ratio	Ref.
MSM β-Ga_2O_3 on sapphire substrate	MBE	0.037@5 V 254 nm	–	–	18%	1.2 nA	–	[9]
MSM β-Ga_2O_3 on sapphire substrate	MBE	> 1.5@4 V 236–240 nm	3.33/0.4 s	–	-	10 nA	$> 10^5$	[16]
MSM β-Ga_2O_3 on sapphire substrate	L-MBE	–	0.86/17.63 s	–	–	128 nA	11	[17]
MSM β-Ga_2O_3 on sapphire substrate	L-MBE	–	0.62/8.97 s	–	–	0.31 nA	-	[18]
MSM β-Ga_2O_3 on bulk Ga_2O_3	L-MBE	0.05@252 nm	0.45/0.24 s	–	–	–	–	[21]
MSM β-Ga_2O_3 on Si	magnetron sputtering	96.13@5 V 250 nm	32.2/78 ms	–	4.76×10^4	1.43 pA	$> 10^3$	[10]
MSM a-GaO_x on sapphire substrate	magnetron sputtering	70.26	0.41/0.02 s	4.76×10^{14}	–	338.6 pA	$> 10^5$	[11]
MSM a-GaO_x on quartz	magnetron sputtering	0.19@20 V 254 nm	80.7/19.1 μs	–	–	–	10^4	[22]
MSM Mg: β-Ga_2O_3 on sapphire substrate	magnetron sputtering	0.024@254 nm	9.17/0.02 s	–	–	4.1 pA	8.7×10^3	[25]
MSM Zn: β-Ga_2O_3 on sapphire substrate	MOCVD	210@232 nm	3.2/1.4 s	–	–	~ pA	8.7×10^4	[23]
MSM Al: β-Ga_2O_3 on sapphire substrate	magnetron sputtering	1.38@5 V 230 nm	3/0.3 s	1.2×10^{13}	551	0.96 pA	–	
MSM Au plasmon β-Ga_2O_3 on Si	magnetron sputtering	50@254 nm	–	–	–	280 nA	–	[28]
MSM Ga/Ga_2O_3 nanocomposite on quartz	magnetron sputtering	2.85@15 V 260 nm	–	–	–	8.52 pA	8×10^5	[29]
MSM exfoliated β-Ga_2O_3 on PET	exfoliated	29.8@254 nm	–	8×10^{12}	–	0.1 pA	8×10^4	[30]
MSM exfoliated β-Ga_2O_3 on Si	exfoliated	1.68@254 nm	1.76/0.53 s	3.73×10^{10}	–	0.28 pA	1.9×10^3	[31]
MSM β-Ga_2O_3 arrays on sapphire	LMBE	0.89@10 V 254 nm	305/251 ms	–	444	10 pA	–	[32]
MSM β-Ga_2O_3 on sapphire	MOCVD	17@20 V 255 nm	–	7×10^{12}	8228	1.85 μA	8.5×10^6	[20]

3. Schottky photodiodes

Schottky photodiodes have many advantages over MSM photodetectors, such as high response speed and possible zero-bias operation due to the built-in electric field, high quantum efficiency, low dark current, and high UV/dark current ratio because of the existence of Schottky barrier. The characteristic of the Schottky photodiodes is the rectifying behavior of the *I*–*V* curve. Usually, a metal is deposited on the surface of the semiconductor, and because of the work function difference of the metal and semiconductor, a Schottky barrier will form in the metal/semiconductor junction. Besides, two kinds of semiconductors are usually put together to form a Schottky junction, and the *I*–*V* characteristics also exhibit rectifying property.

The first solar-blind β-Ga_2O_3 photodiode was reported in 2009 by Rikiya Suzuki *et al.*[33] Au was deposited on single crystal Ga_2O_3 substrate as the Schottky contact. The responsivity of the photodiode was enhanced dramatically after the diode was annealed at 400 °C, leading to a responsivity as high as 10^3 A/W. Chao Yang *et al.*[34] reported a self-powered SBD photodetector based on single crystal Ga_2O_3 substrate with Cu (20 nm) as the Schottky contact and Ti/Au (20 nm/200 nm) as the ohmic contact. The device was annealed at 150 °C in N_2 for 5 min. As shown in Fig. 12(a), the photodiode presented obvious rectifying behavior with a low dark current. Figure 15(b) demonstrated that the device can be operated at zero bias with a peak responsivity at about 250 nm. Xing Chen *et al.*[35] also reported a self-power solar-blind photodetector based on β-Ga_2O_3 nanowires array film with Au as the Schottky contact. They used a simple thermal partial oxidation process to grow β-Ga_2O_3 nanowires on the surface of Ga, which is a very cost-effective and feasible way to make solar-blind Ga_2O_3 photodetector. The key feature of the fabricated Au/β-Ga_2O_3 nanowires photodetector is a very low dark current of 10 pA at −30 V and ultrafast decay time around 64 μs.

In order to improve the responsivity, Daoyou Guo *et al.*[36] combined Nb:$SrTiO_3$ (NSTO) with β-Ga_2O_3 and realized zero-bias operation. The β-Ga_2O_3/NSTO heterojunction based solar-blind photodetector presented a high responsivity of 43.31 A/W and EQE of 2.1×10^4% at the bias voltage of −10 V and 45 μW/cm^2 of 254 nm light illumination. What is more, the device exhibited a fast response time (decay time $\tau_d = 0.07$ s) at zero bias voltage under light illumination of 45 μW/cm^2, which was attributed to the fast separation of photogenerated carriers in the depletion region due to the existence of built-in electric field and then transported to the corresponding electrodes.

Zhenping Wu *et al.*[37] employed lattice compatible semiconductor Ga:ZnO to fabricate β-Ga_2O_3/Ga:ZnO heterojunction based DUV photodetector and the zero-bias operation function was achieved. Figures 12(c) and 12(d) show the *I*–*V* characteristics in the dark and time-dependent photoresponse under 254 nm illumination at 0 V. It can be found that the

β-Ga_2O_3/Ga:ZnO heterojunction based DUV photodetector exhibited obvious rectifying behavior and excellent photoresponse characteristics at zero bias voltage. The peak responsivity of 0.763 mA/W and a fast response speed of 179 ms were obtained under 254 nm illumination. These research works pave a way for high-performance DUV PDs with fast response speed and energy-efficient functionality in the future.

Because of the high thermal and chemical stability of Ga_2O_3, it is a promising candidate for photodetectors working in high temperature. Shihyun Ahn *et al.*[38] evaluated the performance degradation of the Si-implanted β-Ga_2O_3 photodetectors by elevating temperature from 25 °C to 350 °C. The responsivity and EQE were found to increase from 5 A/W to 36 A/W and 2.5×10^3 to 1.75×10^4, respectively, over the temperature range, which was assumed to be caused by the carrier multiplication effect. This result suggests the potential of β-Ga_2O_3 solar-blind photodetectors for high temperature application.

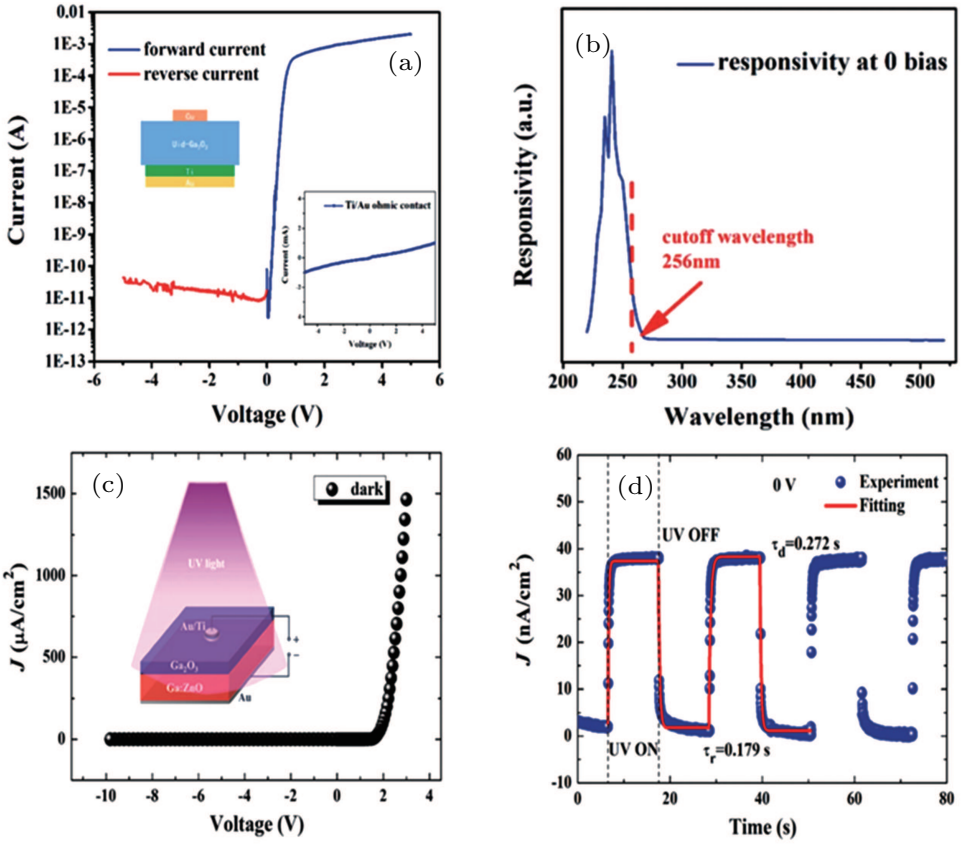


Fig. 12. (a) The *I*–*V* characteristics of the solar-blind Cu/Ga_2O_3 Schottky photodetector in the dark. (b) Photoresponse spectrum of the photodetector at zero bias.[34] (c) The *I*–*V* characteristics of the β-Ga_2O_3/Ga:ZnO heterojunction based photodetector in the dark. The inset shows the schematic figure of the β-Ga_2O_3/Ga:ZnO photodetector. (d) Time-dependent photoresponse characteristics under illumination of 254 nm at 0 V and its corresponding fitting results.[37]

In addition to using metal as the Schottky contact, other semiconductors are also selected to form Schottky junctions. The other wide bandgap materials such as SiC, GaN, ZnO, and diamond were reported to form Schottky heterojunctions with Ga_2O_3, and the heterojunction-based photodiodes showed relatively high photoelectric performance, but still need to be improved. Shinji Nakagomi *et al.*[39] demonstrated a β-Ga_2O_3/SiC heterojunction based deep UV photodiode (Fig. 13(a)) in 2013. The device showed good rectifying behavior and the current was observed to increase abruptly under UV light illumination. Then they reported a deep UV photodiode based on β-Ga_2O_3/GaN heterojunction.[40] As shown in Fig. 13, the current increased linearly with the increase of the deep-UV light intensity. The maximum responsivity of the device was at around 240 nm and the SiC/Ga_2O_3 type photodiode exhibited higher responsivity than the GaN/Ga_2O_3 type one, but with a poor spectral selectivity, as shown in Fig. 13(f). Shinji Nakagomi's works are the initial attempt to combine other wide bandgap materials with Ga_2O_3 to make Schottky photodiodes. The response speed of the devices was reported to be very fast but the responsivity remained low. Yingyu Qu *et al.*[15] reported an enhanced SiC/Ga_2O_3 UV photodetector by replacing the top electrode Ti/Au with single-layer graphene. The device structure and its corresponding photoresponse characteristics are shown in Figs. 13(g)–13(i). The SiC/Ga_2O_3 UV photodetector with graphene as top electrode exhibited higher responsivity of 0.18 A/W and a faster response speed. This work opened up the opportunity for combining graphene with Ga_2O_3 for optoelectronic devices.

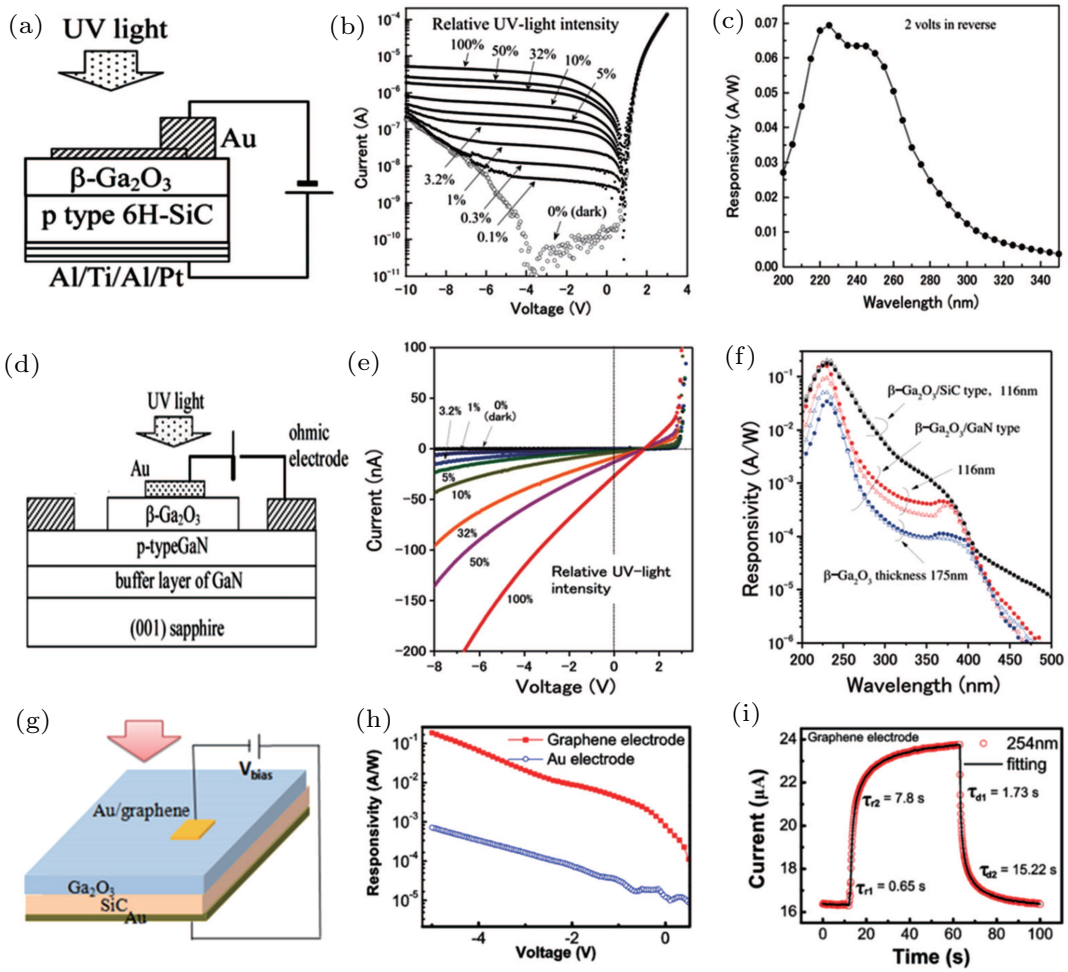


Fig. 13. Device structure of (a) SiC/β-Ga_2O_3 and (d) GaN/β-Ga_2O_3 heterojunction-based photodiodes. The *I–V* characteristics of (b) SiC/Ga_2O_3 and (e) GaN/β-Ga_2O_3 heterojunction-based photodiodes under illumination with different light intensities. Photoresponse spectrum of photodiodes based on (c) β-Ga_2O_3/SiC and (f) GaN/β-Ga_2O_3 heterojunctions.[39,40] (g) Schematic diagram of the SiC/β-Ga_2O_3 UV photodetector with different top electrodes. (h) Responsivity as a function of bias voltage of the SiC/Ga_2O_3 UV photodetector with graphene and Au top electrodes, respectively. (i) Time-dependent photoresponse characteristics of the SiC/Ga_2O_3 UV photodetector with graphene as the top electrode.[15]

Meilin Ai *et al.*[41] reported a graphene/β-Ga_2O_3/graphene sandwich structure UV photodetector with a fast response speed. The fabricated photodetector exhibited good rectifying behavior in the dark and the current increased obviously under 254 nm light illumination (Figs. 14(a) and 14(b)). The fast rise and decay time of the device is 0.96 s and 0.81 s, respectively, as shown in Fig. 14(c). The combination of graphene and Ga_2O_3 opens up a new pathway for the fabrication of Ga_2O_3 optoelectronic devices. Besides, Tao He *et al.*[42] reported a graphene/vertical Ga_2O_3 nanowire array heterojunction-based UV photodetector. The Ga_2O_3 nanowire arrays were obtained from GaN nanowires by thermal oxidization. The graphene/Ga_2O_3 photodetector exhibited a large rejection ratio of 3×10^4 and a fast response speed of 8 ms but a poor responsivity of 0.185 A/W. Wei-Yu Kong *et al.*[14] demonstrated a graphene-β-Ga_2O_3 heterojunction based DUV photodiode by transferring CVD-grown graphene to the surface of the bulk β-Ga_2O_3. From the *I–V* characteristics (Fig. 14(d)), it can be found that the device shows well-defined rectifying behavior. The researchers made a comprehensive study of photoelectric performance dependence on the bias voltage and light intensity. And the responsivity, detectivity, and EQE were found to decrease with increasing light intensity. Specifically, the responsivity, detectivity, and EQE are as high as 39.3 A/W, 5.92×10^{13} Jones, and 1.98×10^4% at 20 V, respectively. However, the rise and decay time is too long (94.83 s and 219.19 s, respectively) because of the severe PPC effect. In order to improve the response speed, Richeng Lin *et al.*[43] transferred the CVD-grown graphene to the β-Ga_2O_3/p-GaN heterojunction substrate and the device exhibited high performance with ultrafast response speed of rise time 1.5 ms and fall time 2 ms due to hot-electron excited carrier multiplication in graphene (Figs. 14(e) and 14(f)). The existence of Schottky barrier in Ga_2O_3/p-GaN and graphene/Ga_2O_3 heterojunctions resulted in the extremely low dark current of 1.25×10^{-8} A/cm^2. And the graphene/β-Ga_2O_3 Schottky junction was advantageous for the separation of photo-generated carriers. The graphene/β-Ga_2O_3 heterojunction DUV photodetector exhibited 1–3 orders of magnitude higher responsivity than the other conventional photodetectors due to a high multiplication gain caused by carrier–carrier scattering in the graphene (Fig. 14(g)).

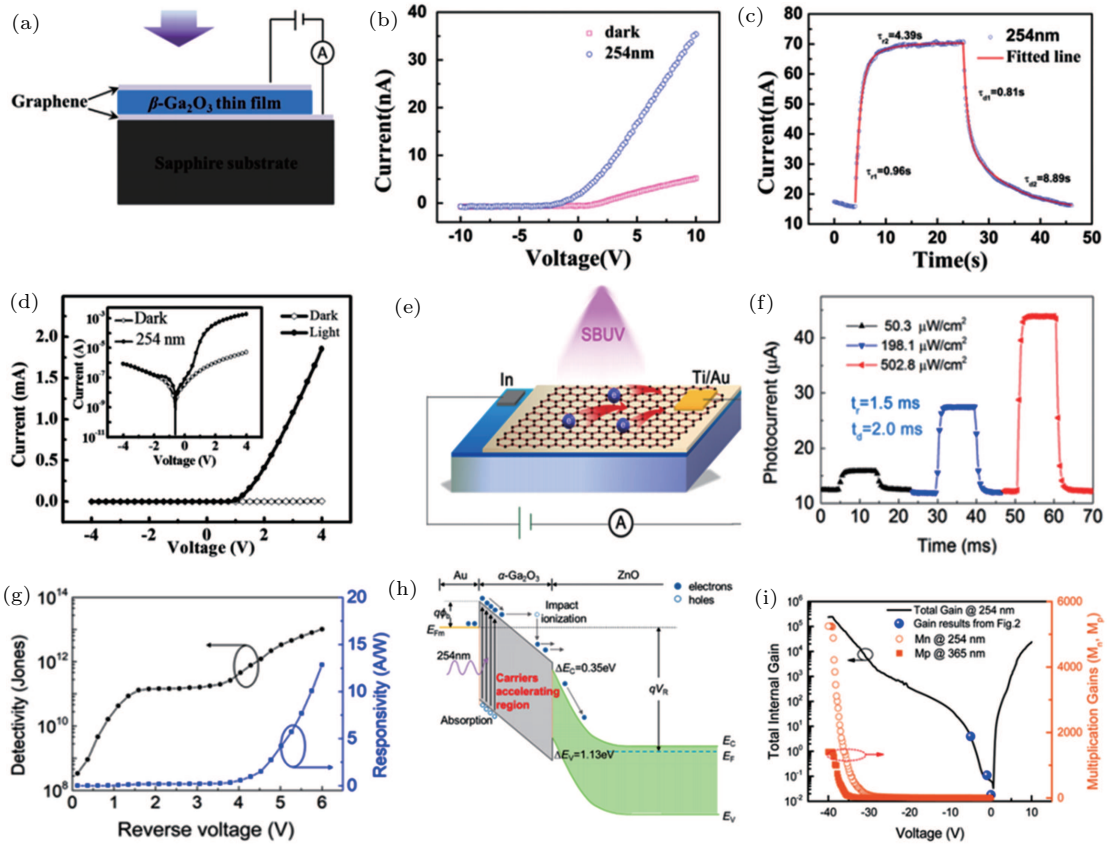


Fig. 14. (a) Schematic of the graphene/β-Ga_2O_3/graphene hybrid structure-based photodiode.[41] (b) *I–V* characteristics of the graphene/β-Ga_2O_3/graphene hybrid structure-based photodiode in the dark and under light illumination of 254 nm.[41] (c) Time-dependent photoresponse of the graphene/β-Ga_2O_3/graphene hybrid structure-based photodiode.[41] (d) *I–V* curves of the graphene-β-Ga_2O_3 heterojunction-based DUV photodiode in the dark and under 254 nm light illumination.[14] (e) Schematic figure of graphene/Ga_2O_3/p-GaN heterojunction-based photodiode.[43] (f) Time-dependent photoresponse characteristics of the graphene/Ga_2O_3/p-GaN heterojunction-based photodiode.[43] (g) Detectivity and responsivity as a function of bias voltage of the graphene/Ga_2O_3/p-GaN heterojunction-based photodiode.[43] (h) Schematic energy diagram of the α-Ga_2O_3/ZnO heterojunction at high reverse bias voltage under illumination of 254 nm.[12] (i) Photoconductive gain of the α-Ga_2O_3/ZnO heterojunction-based solar-blind photodetector as a function of bias voltage under 254 nm and 365 nm illumination.[12]

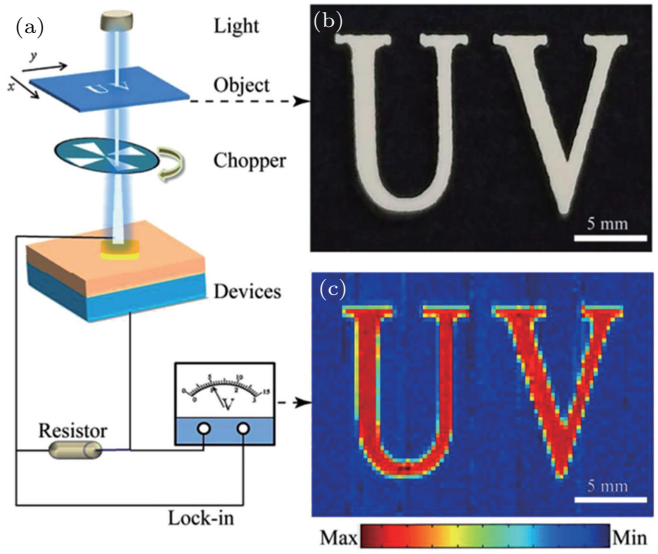


Fig. 15. (a) Schematic presentation of the imaging system by using the diamond/β-Ga_2O_3 heterojunction-based solar-blind photodetector as the sensing pixel at bias voltage of 0 V. (b) The imaged object with letters of "UV" on a black paper. (c) The image obtained from the imaging system.[13]

Schottky photodiodes usually exhibit high response speed but lower responsivity. Daoyou Guo *et al.*[44] tried to combine ZnO with β-Ga_2O_3 and fabricated ZnO/β-Ga_2O_3 heterojunction-based UV photodetector. The zero-bias operation functionality was achieved but the responsivity of 0.35 A/W remained too low. The avalanche photodiode is an ideal candidate to break the trade-off between the responsivity and response speed. Xuanhu Chen *et al.*[12] reported a method of combining ZnO with α-Ga_2O_3 to make solar-blind photodetector with high avalanche gain. LMBE was used to deposit the α-Ga_2O_3 thin film on ZnO. The energy diagram and photoconductive gain of the device are shown in Figs. 14(h) and 14(i). The device can achieve zero-bias function with a low dark current of 1 pA, a UV/visible rejection ratio of 10^3, and a detectivity of 9.66×10^{12} Jones. Specifically, high total gain over 10^5 and ultrahigh responsivity of 1.10×10^4 were achieved, caused by avalanche multiplication processes. Such α-Ga_2O_3/ZnO heterojunction based solar-blind photodetector with high performance has great potential for future application.

There are some works based on ZnO-Ga_2O_3 core-shell heterojunction microwire to make solar-blind photodetectors.[45,46] In Ref. [46], the CVD grown ZnO-

Ga_2O_3 core-shell microwire was transferred to PET substrate, and piezo-phototronic effect of ZnO was utilized to enhance the UV photocurrent response by about three times under −0.042% static strain. Bin Zhao *et al.*[45] also used CVD approach to grow the ZnO-Ga_2O_3 core-shell microwire and the heterojunction showed good rectifying behavior according to the *I*–*V* characteristics. The device exhibited high UV/visible rejection ratio ($R_{251\ nm}/R_{400\ nm}$) of 6.9×10^2 under zero bias. What is more, the self-powered photodetector showed ultrahigh response speed with rise time of 100 μs and decay time of 900 μs. In short, the microstructure junction provides a new design way to achieve high performance solar-blind photodetector.

Besides, Yan-Cheng Chen *et al.*[13] made a self-powered diamond/β-Ga_2O_3 photodetectors, and for the first time, they reported on solar-blind imaging of Ga_2O_3 based photodetectors, as shown in Fig. 15. The device showed a high UV/visible rejection ratio, but the responsivity remained too low, only 0.2 mA/W. The picture obtained from the imaging system showed sharp boundaries, indicating that the imaging system has high fidelity characteristics and is potential for future imaging application. Table 4 summarizes the key performance parameters of Schottky-type Ga_2O_3 photodiodes reported in recent years.

Table 4. Comparison of key figures-of-merit of recent Ga_2O_3 based Schottky photodiodes.

Materials and structures	Growth method	R/A·W^{-1}	τ_r/τ_d	D^*/Jones	EQE/%	Dark current	UV/dark rejection ratio	Ref.
Au/β-Ga_2O_3 photodiode	bulk	10^3@240 nm	–	–	–	–	–	[33]
Cu/β-Ga_2O_3 photodiode	bulk	–	0.729/1.209 s	–	–	–	5×10^7	[34]
Au/β-Ga_2O_3 nanoarray film	thermal oxidation	2.9@–50 V 254 nm	1/64 μs	–	–	10 pA	–	[35]
β-Ga_2O_3/NSTO photodiode	magnetron sputtering	43.31@–10 V 254 nm	0.07 s	–				
β-Ga_2O_3/Ga:ZnO photodiode	LMBE	0.763 mA/W@254 nm	0.179/0.272 s	–	–	0.15 nA·cm^{-2}	10^2	[37]
β-Ga_2O_3/GaN photodiode	–	0.18@225 nm	0.3 ms	–	–	1 nA	-	[40]
Graphene/β-Ga_2O_3/SiC photodiode	LMBE	0.18@254 nm	0.65/1.73 s	–	–	0.5 nA	63.31	[15]
Graphene/β-Ga_2O_3/graphene photodiode	LMBE	9.66@10 V 254 nm	0.96/0.81 s	–	–	∼ nA	82.88	[41]
Graphene/vertical Ga_2O_3 nanowire array photodiode	thermal oxidation	0.185@–5 V 258 nm	9/8 ms	–	–	1.14 μA	3×10^4	[42]
Graphene/β-Ga_2O_3 photodiode	bulk	39.3@20 V 254 nm	94.83/219.19 s	5.92×10^{13}	1.98×10^4%	1.1 μA	–	[14]
Graphene/β-Ga_2O_3 photodiode	MOCVD	12.8@6v 254 nm	1.5/2 ms	1.3×10^{13}	–	12.5 nA·cm^{-2}	–	[43]
β-Ga_2O_3/ZnO photodiode	Magnetron sputtering	0.35@–5 V 254 nm	0.62/0.67 s	–	1.75×10^2%	0.29 nA	14.8	[44]
α-Ga_2O_3 /ZnO photodiode	LMBE	0.5@–5 V 255 nm	238 μs/3.04 ms	9.66×10^{12}	–	1 pA	10^3	[12]
ZnO/Ga_2O_3 core–shell microwire	CVD	9.7 mA/W@251 nm	1/9 ms	6.29×10^{12}	–	–	6.9×10^2	[45]
Diamond/β-Ga_2O_3 photodiode	PECVD	2×10^{-4}@0 V 244 nm	–	6.9×10^9	–	2.6 nA·cm^{-2}	37	[13]

4. Conclusions and perspectives

We have reviewed the research works on Ga_2O_3 based solar-blind photodetectors reported in recent years. Great achievements were realized. The classification, mechanism, and performance of different photodetectors have been summarized. The Ga_2O_3 based solar-blind photodetectors are now mainly based on two structures: MSM and Schottky diode. MSM structure based Ga_2O_3 photodetectors have the advantages of easy-fabrication and integration and their performances are dependent on the size of the interdigital electrodes. The Ga_2O_3 Schottky diodes exhibit high response speed and high rejection ratio. Different kinds of metals were used to form Schottky contact with Ga_2O_3, and other wide bandgap materials such as SiC, GaN, ZnO, and diamond were also employed to form heterojunction with Ga_2O_3. Good rectifying characteristics were achieved in these devices. Besides, graphene was used to form Schottky contact with Ga_2O_3, and the photodetectors exhibited high performance. The photoelectric performance of the Ga_2O_3 solar-blind photodetector is not only dependent on the device structure but also dependent on the quality of the Ga_2O_3. At the beginning, the Ga_2O_3 solar-blind photodetectors were based on single crystal bulk or thin film β-Ga_2O_3. Different nano-optoelectronic devices have been reported to detect DUV light using exfoliated Ga_2O_3 nano-flakes. These devices also exhibited excellent DUV photodetection characteristics, such as fast switching speed and high responsivity. The combination of exfoliated Ga_2O_3 nano-flakes and 2D materials opens up a way for novel functional nano-devices. Amorphous Ga_2O_3 based solar-blind photodetectors are being paid more and more at-

tention due to their cost-effective, easy-fabrication process and high performance in certain aspects. By optimizing the growth condition, amorphous Ga_2O_3 thin film based Ga_2O_3 photodetectors are potential for the practical application in the future. Although great progress has been made in Ga_2O_3 photodetectors, the responsivity remains too low to be applicated practically. Much more efforts need to be made to improve the responsivity, EQE, and the response speed at the same time. Besides, p-type doping of Ga_2O_3 is still a bottleneck problem which severely limits its application in the optoelectronic system. Furthermore, the severe persistent photoconductivity effect, which is common in oxide, needs to be addressed. In addition, for further practical application, the imaging and ultraviolet light communication based on Ga_2O_3 photodetectors deserve to be more insensitively explored.

References

[1] Chen H, Liu K, Hu L, Al-Ghamdi A A and Fang X 2015 *Mater. Today* **18** 493
[2] Razeghi M 2002 *Proc. IEEE* **90** 1006
[3] Sang L, Liao M and Sumiya M 2013 *Sensors* **13** 10482
[4] Razeghi M and Rogalski A 1996 *J. Appl. Phys.* **79** 7433
[5] Muñoz E, Monroy E, Pau J L, Calle F, Omnès F and Gibart P 2001 *J. Phys.: Condens. Matter* **13** 7115
[6] Yu-Zung C and Jing-Jou T 2004 *Jpn. J. Appl. Phys.* **43** 4146
[7] Fan M M, Liu K W, Zhang Z Z, Li B H, Chen X, Zhao D X, Shan C X and Shen D Z 2014 *Appl. Phys. Lett.* **105** 011117
[8] Kokubun Y, Miura K, Endo F and Nakagomi S 2007 *Appl. Phys. Lett.* **90** 031912
[9] Takayoshi O, Takeya O and Shizuo F 2007 *Jpn. J. Appl. Phys.* **46** 7217
[10] Arora K, Goel N, Kumar M and Kumar M 2018 *ACS Photon.* **5** 2391
[11] Qian L X, Wu Z H, Zhang Y Y, Lai P T, Liu X Z and Li Y R 2017 *ACS Photon.* **4** 2203
[12] Chen X, Xu Y, Zhou D, Yang S, Ren F F, Lu H, Tang K, Gu S, Zhang R, Zheng Y and Ye J 2017 *ACS Appl. Mater. & Interfaces* **9** 36997
[13] Chen Y C, Lu Y J, Lin C N, Tian Y Z, Gao C J, Dong L and Shan C X 2018 *J. Mater. Chem. C* **6** 5727
[14] Kong W Y, Wu G A, Wang K Y, Zhang T F, Zou Y F, Wang D D and Luo L B 2016 *Advanced Mater.* **28** 10725
[15] Qu Y, Wu Z, Ai M, Guo D, An Y, Yang H, Li L and Tang W 2016 *J. Alloys Compd.* **680** 247
[16] A Singh Pratiyush, Krishnamoorthy S, S Vishnu Solanke, Xia Z, Muralidharan R, Rajan S and Nath D N 2017 *Appl. Phys. Lett.* **110** 221107
[17] Guo D, Wu Z, Li P, An Y, Liu H, Guo X, Yan H, Wang G, Sun C, Li L and Tang W 2014 *Opt. Mater. Express* **4** 1067
[18] Guo D Y, Wu Z P, An Y H, Guo X C, Chu X L, Sun C L, Li L H, Li P G and Tang W H 2014 *Appl. Phys. Lett.* **105** 023507
[19] Huang C Y, Horng R H, Wuu D S, Tu L W and Kao H S 2013 *Appl. Phys. Lett.* **102** 011119
[20] Hu G C, Shan C X, Zhang N, Jiang M M, Wang S P and Shen D Z 2015 *Opt. Express* **23** 13554
[21] Feng Q, Huang L, Han G, Li F, Li X, Fang L, Xing X, Zhang J, Mu W, Jia Z, Guo D, Tang W, Tao X and Hao Y 2016 *IEEE Trans. Electron. Devices* **63** 3578
[22] Cui S, Mei Z, Zhang Y, Liang H and Du X 2017 *Advanced Opt. Mater.* **5** 1700454
[23] Alema F, Hertog B, Ledyaev O, Volovik D, Thoma G, Miller R, Osinsky A, Mukhopadhyay P, Bakhshi S, Ali H and Schoenfeld W V 2017 *Phys. Status Solidi (a)* **214** 1600688
[24] Ma X, Zhang Y, Dong L and Jia R 2017 *Results Phys.* **7** 1582
[25] Qian Y P, Guo D Y, Chu X L, Shi H Z, Zhu W K, Wang K, Huang X K, Wang H, Wang S L, Li P G, Zhang X H and Tang W H 2017 *Mater. Lett.* **209** 558
[26] Feng Q, Li X, Han G, Huang L, Li F, Tang W, Zhang J and Hao Y 2017 *Opt. Mater. Express* **7** 1240
[27] Yuan S, Wang C, Huang S and Wuu D 2018 *IEEE Electron Device Lett.* **39** 220
[28] An Y, Chu X, Huang Y, Zhi Y, Guo D, Li P, Wu Z and Tang W 2016 *Prog. Nat. Sci.: Mater. Int.* **26** 65
[29] Cui S J, Mei Z X, Hou Y N, Chen Q S, Liang H L, Zhang Y H, Huo W X and Du X L 2018 *Chin. Phys. B* **27** 067301
[30] Oh S, Kim C K and Kim J 2018 *ACS Photon.* **5** 1123
[31] Oh S, Mastro M A, Tadjer M J and Kim J 2017 *ECS J. Solid State Sci. Technol.* **6** Q79–Q83
[32] Peng Y, Zhang Y, Chen Z, Guo D, Zhang X, Li P, Wu Z and Tang W 2018 *IEEE Photon. Technol. Lett.* **30** 993
[33] Suzuki R, Nakagomi S, Kokubun Y, Arai N and Ohira S 2009 *Appl. Phys. Lett.* **94** 222102
[34] Yang C, Liang H, Zhang Z, Xia X, Tao P, Chen Y, Zhang H, Shen R, Luo Y and Du G 2018 *RSC Adv.* **8** 6341
[35] Chen X, Liu K, Zhang Z, Wang C, Li B, Zhao H, Zhao D and Shen D 2016 *ACS Appl. Mater. & Interfaces* **8** 4185
[36] Guo D, Liu H, Li P, Wu Z, Wang S, Cui C, Li C and Tang W 2017 *ACS Appl. Mater. & Interfaces* **9** 1619
[37] Wu Z, Jiao L, Wang X, Guo D, Li W, Li L, Huang F and Tang W 2017 *J. Mater. Chem. C* **5** 8688
[38] Ahn S, Ren F, Oh S, Jung Y, Kim J, Mastro M A, Hite J K, Eddy C R and Pearton S J 2016 *J. Vac. Sci. & Technol. B* **34** 041207
[39] Nakagomi S, Momo T, Takahashi S and Kokubun Y 2013 *Appl. Phys. Lett.* **103** 072105
[40] Nakagomi S, Sato T A, Takahashi Y and Kokubun Y 2015 *Sensors Actuators A: Phys.* **232** 208
[41] Ai M, Guo D, Qu Y, Cui W, Wu Z, Li P, Li L and Tang W 2017 *J. Alloys Compd.* **692** 634
[42] He T, Zhao Y, Zhang X, Lin W, Fu K, Sun C, Shi F, Ding X, Yu G, Zhang K, Lu S, Zhang X and Zhang B 2018 *Nano Photon.* **7** 1557
[43] Lin R, Zheng W, Zhang D, Zhang Z, Liao Q, Yang L and Huang F 2018 *ACS Appl. Mater. & Interfaces* **10** 22419
[44] Guo D Y, Shi H Z, Qian Y P, Lv M, Li P G, Su Y L, Liu Q, Chen K, Wang S L, Cui C, Li C R and Tang W H 2017 *Semiconductor Sci. Technol.* **32** 03LT01
[45] Zhao B, Wang F, Chen H, Zheng L, Su L, Zhao D and Fang X 2017 *Advanced Funct. Mater.* **27** 1700264
[46] Chen M, Zhao B, Hu G, Fang X, Wang H, Wang L, Luo J, Han X, Wang X, Pan C and Wang Z L 2018 *Advanced Funct. Mater.* **28** 1706379